

Human-specific *ARHGAP11B* induces hallmarks of neocortical expansion in developing ferret neocortex

Nereo Kalebic, Carlotta Gilardi, Mareike Albert, Takashi Namba, Katherine R Long, Milos Kostic, Barbara Langen, Wieland B Huttner*

Max Planck Institute of Molecular Cell Biology and Genetics, Dresden, Germany

Abstract The evolutionary increase in size and complexity of the primate neocortex is thought to underlie the higher cognitive abilities of humans. *ARHGAP11B* is a human-specific gene that, based on its expression pattern in fetal human neocortex and progenitor effects in embryonic mouse neocortex, has been proposed to have a key function in the evolutionary expansion of the neocortex. Here, we study the effects of *ARHGAP11B* expression in the developing neocortex of the gyrencephalic ferret. In contrast to its effects in mouse, *ARHGAP11B* markedly increases proliferative basal radial glia, a progenitor cell type thought to be instrumental for neocortical expansion, and results in extension of the neurogenic period and an increase in upper-layer neurons. Consequently, the postnatal ferret neocortex exhibits increased neuron density in the upper cortical layers and expands in both the radial and tangential dimensions. Thus, human-specific *ARHGAP11B* can elicit hallmarks of neocortical expansion in the developing ferret neocortex.

DOI: <https://doi.org/10.7554/eLife.41241.001>

Introduction

The expansion of the neocortex during primate evolution is thought to constitute one important basis for the unparalleled cognitive abilities of humans. The size of the neocortex is mainly regulated by the proliferative capacity of neural progenitor cells during cortical development and the length of the neurogenic period (Azevedo et al., 2009; Borrell and Götz, 2014; Dehay et al., 2015; Kaas, 2013; Kalebic et al., 2017; Krubitzer, 2007; Lui et al., 2011; Molnár et al., 2006; Rakic, 2009; Sousa et al., 2017; Wilsch-Bräuninger et al., 2016).

Two major classes of neural progenitors can be distinguished: apical progenitors (APs), whose cell bodies reside in the ventricular zone (VZ), and basal progenitors (BPs), whose cell bodies reside in the subventricular zone (SVZ). Whereas APs are highly proliferative in the neocortex of all mammalian species studied (Götz and Huttner, 2005; Rakic, 2003a), BPs are highly proliferative only in species with an expanded neocortex (Borrell and Götz, 2014; Florio and Huttner, 2014; Lui et al., 2011; Reillo et al., 2011). Specifically, a subtype of BPs, called basal (or outer) radial glia (bRG), are thought to play a key role in the evolutionary expansion of the neocortex (Borrell and Götz, 2014; Florio and Huttner, 2014; Lui et al., 2011). Importantly, in species with an expanded neocortex, such as primates or the ferret, the SVZ has been shown to be divided into two distinct histological zones: the inner and outer SVZ (ISVZ and OSVZ, respectively) (Dehay et al., 2015; Reillo and Borrell, 2012; Smart et al., 2002). The OSVZ is uniquely important for the evolutionary expansion of the neocortex, as proliferative bRG are particularly abundant in this zone (Betizeau et al., 2013; Fietz et al., 2010; Hansen et al., 2010; Poluch and Juliano, 2015; Reillo and Borrell, 2012; Reillo et al., 2011; Smart et al., 2002). Increased proliferative capacity of bRG results in an amplification of BP number and is accompanied by a prolonged phase of production of late-born neurons

*For correspondence: huttner@mpi-cbg.de

Competing interests: The authors declare that no competing interests exist.

Funding: See page 21

Received: 19 August 2018

Accepted: 23 November 2018

Published: 28 November 2018

Reviewing editor: Paola Arlotta, Harvard University, United States

© Copyright Kalebic et al. This article is distributed under the terms of the [Creative Commons Attribution License](https://creativecommons.org/licenses/by/4.0/), which permits unrestricted use and redistribution provided that the original author and source are credited.

eLife digest The human brain owes its characteristic wrinkled appearance to its outer layer, the cerebral cortex. All mammals have a cerebral cortex, but its size varies greatly between species. As the brain evolved, the neocortex, the evolutionarily youngest part of the cerebral cortex, expanded dramatically and so had to fold into wrinkles to fit inside the skull. The human neocortex is roughly three times bigger than that of our closest relatives, the chimpanzees, and helps support advanced cognitive skills such as reasoning and language. But how did the human neocortex become so big?

The answer may lie in genes that are unique to humans, such as *ARHGAP11B*. Introducing *ARHGAP11B* into the neocortex of mouse embryos increases its size and can induce folding. It does this by increasing the number of neural progenitors, the cells that give rise to neurons. But there are two types of neural progenitors in mammalian neocortex: apical and basal. A subtype of the latter – basal radial glia – is thought to drive neocortex growth in human development. Unfortunately, mice have very few basal radial glia. This makes them unsuitable for testing whether *ARHGAP11B* acts via basal radial glia to enlarge the human neocortex.

Kalebic et al. therefore introduced *ARHGAP11B* into ferret embryos in the womb. Ferrets have a larger neocortex than mice and possess more basal radial glia. Unlike in mice, introducing this gene into the ferret neocortex markedly increased the number of basal radial glia. It also extended the time window during which the basal radial glia produced neurons. These changes increased the number of neurons, particularly of a specific subtype found mainly in animals with large neocortex and thought to be involved in human cognition.

Introducing human-specific *ARHGAP11B* into embryonic ferrets thus helped expand the ferret neocortex. This suggests that this gene may have a similar role in human brain development. Further experiments are needed to determine whether ferrets with the *ARHGAP11B* gene, and thus a larger neocortex, have enhanced cognitive abilities. If they do, testing these animals could provide insights into human cognition. The animals could also be used to model human brain diseases and to test potential treatments.

DOI: <https://doi.org/10.7554/eLife.41241.002>

(Geschwind and Rakic, 2013; Otani et al., 2016; Rakic, 2009). As the mammalian cerebral cortex is generated in an inside-out fashion, these late-born neurons occupy the upper-most layers of the cortex (Lodato and Arlotta, 2015; Molnár et al., 2006; Molyneaux et al., 2007; Rakic, 1972; Rakic, 2009; Sidman and Rakic, 1973). Thus, an increased generation of upper-layer neurons and increased thickness of the upper layers are also hallmarks of an expanded neocortex.

The evolutionary expansion of the neocortex is characteristically accompanied by an increase in the abundance of proliferative bRG, in the length of the neurogenic period, and in the relative proportion of upper-layer neurons within the cortical plate (Borrell and Götz, 2014; Dehay et al., 2015; Florio and Huttner, 2014; Geschwind and Rakic, 2013; Lui et al., 2011; Molnár et al., 2006; Sousa et al., 2017; Wilsch-Bräuninger et al., 2016). This is most obvious when comparing extant rodents, such as mouse, with primates, such as human. Carnivores, such as ferret, display intermediate features (Borrell and Reillo, 2012; Hutsler et al., 2005; Kawasaki, 2014; Reillo et al., 2011). Specifically, ferrets exhibit a gyrified neocortex and, during development, a pronounced OSVZ populated with proliferative bRG (Barnette et al., 2009; Borrell and Reillo, 2012; Fietz et al., 2010; Kawasaki, 2014; Kawasaki et al., 2013; Poluch and Juliano, 2015; Reillo et al., 2011; Sawada and Watanabe, 2012; Smart and McSherry, 1986a; Smart and McSherry, 1986b). In this context, it should be noted that in evolution, the split between the lineages leading to mouse and to human occurred a few million years later than that leading to ferret and human (Bininda-Emonds et al., 2007).

In addition to the above-mentioned features associated with neocortex expansion in general, certain specific aspects of human neocortex expansion are thought to involve human-specific genomic changes. Recent transcriptomic studies established that certain previously identified human-specific genes (Bailey et al., 2002; Dennis and Eichler, 2016) are preferentially expressed in neural progenitor cells and have implicated these genes in human neocortex expansion (Fiddes et al., 2018; Florio et al., 2015; Florio et al., 2018; Florio et al., 2016; Suzuki et al., 2018). Among these

genes, the one that showed the most specific expression in human bRG compared to neurons was *ARHGAP11B* (Florio *et al.*, 2015). *ARHGAP11B* arose in evolution after the split of the human lineage from the chimpanzee lineage, as a product of a partial gene duplication of *ARHGAP11A*, a gene encoding a Rho GTPase activating protein (Dennis *et al.*, 2017; Florio *et al.*, 2015; Florio *et al.*, 2016; Kagawa *et al.*, 2013). Forced expression of *ARHGAP11B* in the embryonic mouse neocortex leads to an increase in BP proliferation and pool size (Florio *et al.*, 2015). However, as described above, the mouse exhibits only a minute amount of bRG, a cell type thought to be instrumental for neocortex expansion, and the role of *ARHGAP11B* on the pool size of bRG, therefore, remains elusive. Additionally, the role of *ARHGAP11B* on the production of upper-layer neurons, another hallmark of the evolutionary expansion of the neocortex, is also unknown. Here, we study the effects of forced expression of *ARHGAP11B* in the developing ferret neocortex, which already exhibits several features of an expanded neocortex, including an abundance of bRG and of upper-layer neurons, and as such is a suitable model organism to address the role of *ARHGAP11B* in the evolutionary expansion of the neocortex.

Results

We expressed *ARHGAP11B* in the ferret neocortex starting at embryonic day 33 (E33), when both the generation of upper-layer neurons and formation of the OSVZ start (Martínez-Martínez *et al.*, 2016). Specifically, we performed *in utero* electroporation of ferrets (Kawasaki *et al.*, 2012; Kawasaki *et al.*, 2013) at E33 with a plasmid encoding *ARHGAP11B* under the constitutive CAG promoter or an empty vector as control. The analyses of electroporated embryos were performed at four different developmental stages: E37, E40/postnatal day (P) 0, 10 and 16 (Figure 1—figure supplement 1A). To be able to visualize the electroporated area, we co-electroporated *ARHGAP11B*-expressing and control plasmids with vectors encoding fluorescent markers. For postnatal studies, to be able to distinguish the electroporated kits, the *ARHGAP11B*-expressing plasmid was co-electroporated with a GFP-encoding plasmid, and the control vector with an mCherry-encoding plasmid, or vice versa. For the sake of simplicity, we refer to both fluorescent markers as Fluorescent Protein (FP) from here onwards, and both FPs are depicted in green color in all figures.

We detected *ARHGAP11B* transcript by RT-qPCR at all the stages analyzed and only in ferret embryos/kits subjected to *ARHGAP11B in utero* electroporation (Figure 1—figure supplement 1B–D). Additionally, immunofluorescence at E37 demonstrated the specific presence of the *ARHGAP11B* protein in neural progenitors of such embryos (Figure 1—figure supplement 1E,F and see Materials and methods for details).

ARHGAP11B increases the abundance of BPs in the developing ferret neocortex

We first examined the ability of *ARHGAP11B* to increase BP abundance in ferret. To this end, we immunostained E40/P0 ferret neocortex for PCNA, a marker of cycling cells, in order to identify progenitor cells (Figure 1A and Figure 1—figure supplement 2A). We observed an increase in the proportion of PCNA+ FP+ cells in OSVZ of the *ARHGAP11B*-expressing embryos compared to control (Figure 1B). The abundance of PCNA+ FP+ cells was increased in both ISVZ and OSVZ, but this increase was particularly strong in the OSVZ (Figure 1—figure supplement 2B). Of note, we did not detect any increase in the abundance of FP– progenitor cells in the SVZ, suggesting that *ARHGAP11B* does not promote any non-cell-autonomous effects (Figure 1—figure supplement 2C).

We next immunostained the E40/P0 ferret neocortex for phospho-vimentin (PhVim), a marker of mitotic cells (Figure 1C). Our analysis revealed no effect of *ARHGAP11B* expression on apical mitoses (Figure 1D, left-most) and on basal mitoses in the abventricular VZ (Figure 1D, second column from left) compared to control. In contrast, a 3-fold increase in the abundance of basal mitotic cells in the SVZ was detected (Figure 1D, sum of ISVZ and OSVZ). This increase was observed for the ISVZ (2-fold, Figure 1D, second column from right), but was especially prominent for the OSVZ (5-fold, Figure 1D, right-most column). A comparably large increase (5-fold) was detected when examining mitotic bRG, that is, PhVim+ BPs exhibiting a PhVim+ process in the OSVZ (Figure 1E,F). bRG accounted for ≈50% of all BPs upon *ARHGAP11B* expression, and their relative proportion was not significantly changed compared to control or non-electroporated regions (Figure 1—figure supplement 2D). Of note, this strong increase in FP+ basal mitoses was not accompanied by any change in

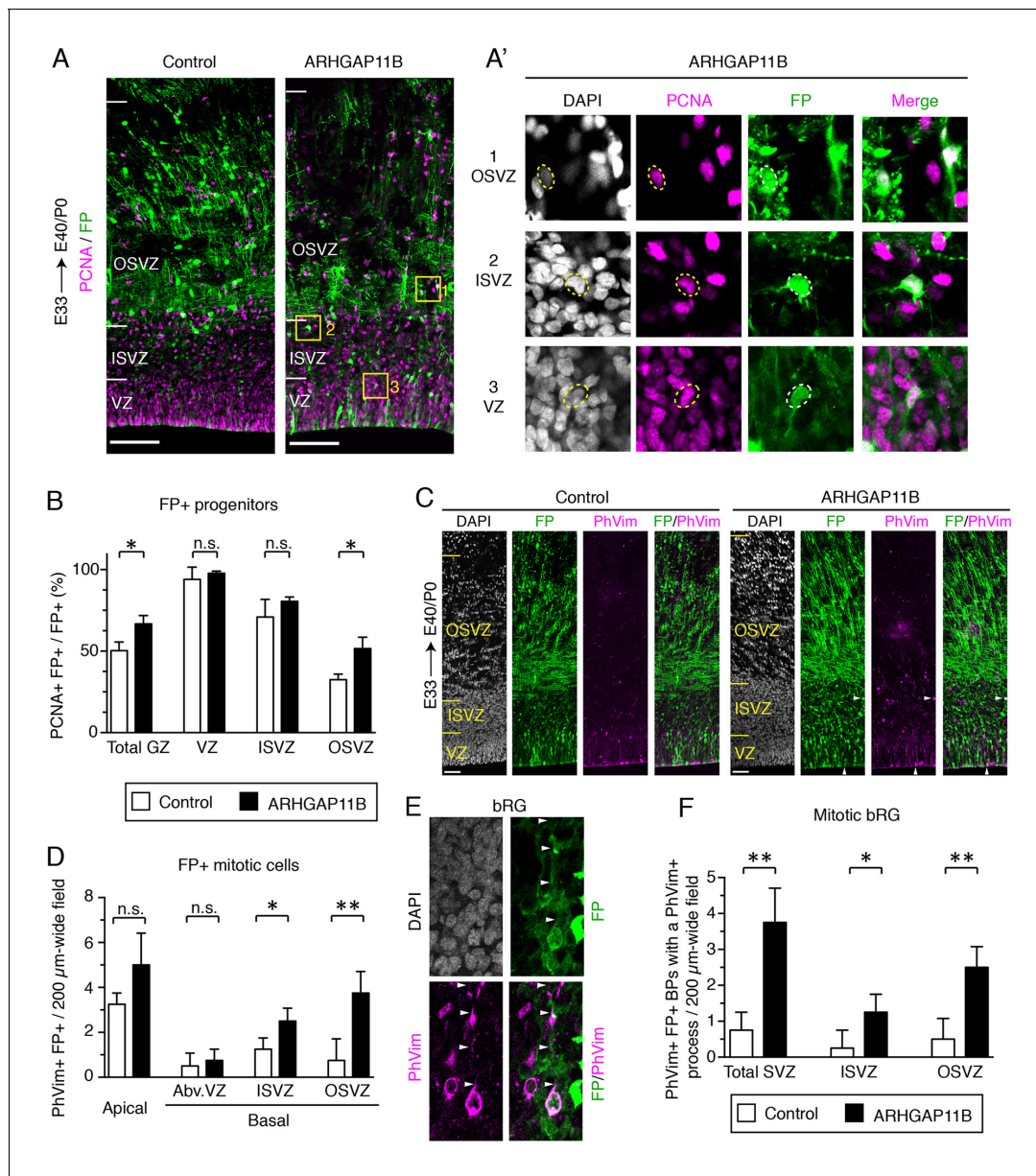


Figure 1. ARHGAP11B increases the abundance of BPs in the developing ferret neocortex. Ferret E33 neocortex was electroporated *in utero* with a plasmid encoding a fluorescent protein (FP) together with either a plasmid encoding ARHGAP11B or empty vector (Control), followed by analysis at E40/P0. (A) Double immunofluorescence for FP (green) and PCNA (magenta) (for the images of the single channels and DAPI staining, see **Figure 1—figure supplement 2A**). Images are single optical sections. Scale bars, 100 μm . Boxes (50 \times 50 μm) indicate FP+ BPs in the OSVZ (1, top), ISVZ (2, middle) and VZ (3, bottom), shown at higher magnification in (A'). (A') Dashed lines indicate a cell body contour. (B) Percentage of FP+ cells in the germinal zones (GZ total) and in the VZ, ISVZ and OSVZ that are PCNA+ upon control (white) and ARHGAP11B (black) electroporations. Data are the mean of 3 experiments. Error bars indicate SD; *, $p < 0.05$; n.s., not statistically significant; Student's *t*-test. (C) Double immunofluorescence for FP (green) and phospho-vimentin (PhVim, magenta), combined with DAPI staining (white). Images are single optical sections. Scale bars, 50 μm . Vertical arrowheads, apical mitosis; horizontal arrowheads, basal mitosis. (D) Quantification of FP+ mitotic cells, as revealed by PhVim immunofluorescence, in a 200 μm -wide field of the cortical wall, upon control (white) and ARHGAP11B (black) electroporations. Apical, mitoses lining the ventricular surface; basal, mitoses away from the ventricle (Abv.VZ, abventricular VZ; ISVZ; OSVZ). Data are the mean of 4 experiments. Error bars indicate SD; **, $p < 0.01$; *, $p < 0.05$; n.s., not statistically significant; Student's *t*-test. (E) Mitotic bRG (single optical sections). Double immunofluorescence for FP (green) and phospho-vimentin (PhVim, magenta), combined with DAPI staining (white), upon electroporation of the plasmid encoding FP together with the plasmid encoding ARHGAP11B. Arrowheads, PhVim+ basal process of the mitotic bRG. Images are oriented with the apical side facing down and are 25 μm wide. (F) Quantification of mitotic bRG (FP+ PhVim+ cell bodies in the SVZ that contain a PhVim+ process), in a 200 μm -wide field of total SVZ (left), ISVZ (middle) and OSVZ (right), upon control (white) and ARHGAP11B (black) electroporations. Data are the mean of 4 experiments. Error bars indicate SD; **, $p < 0.01$; *, $p < 0.05$; Student's *t*-test.

Figure 1 continued on next page

Figure 1 continued

DOI: <https://doi.org/10.7554/eLife.41241.003>

The following figure supplements are available for figure 1:

Figure supplement 1. Forced expression of ARHGAP11B in the developing ferret neocortex.

DOI: <https://doi.org/10.7554/eLife.41241.004>

Figure supplement 2. ARHGAP11B increases the abundance of BPs in the developing ferret neocortex.

DOI: <https://doi.org/10.7554/eLife.41241.005>

FP+ mitotic cells (**Figure 1—figure supplement 2E**) nor by a change in thickness of the ferret germinal zones (**Figure 1—figure supplement 2F**). Taken together, these data indicate that ARHGAP11B markedly increases the abundance of BP, in particular bRG, when expressed in the embryonic ferret neocortex.

ARHGAP11B increases the proportion of Sox2-positive bRG that are Tbr2-negative

We next analyzed the ARHGAP11B-increased bRG in more detail. Proliferative neural progenitors, in particular apical radial glia (aRG) and bRG, characteristically express the transcription factor Sox2 (**Pollen et al., 2015**). We therefore immunostained E40/P0 ferret neocortex for Sox2 (**Figure 2A**) and detected a 40% increase in the proportion of Sox2+ FP+ cells in the germinal zones (GZs) (**Figure 2B**). This increase was exclusively due to an increase in BPs, as we observed a doubling of the proportion of Sox2+ FP+ cells in both the ISVZ and OSVZ, but no increase in the VZ (**Figure 2C**), upon ARHGAP11B expression. These data in turn are consistent with the effects of ARHGAP11B described above (**Figure 1—figure supplement 2B**).

We then analyzed the FP+ cells for the expression of the transcription factor Tbr2 (**Figure 2A**), a marker of certain BPs (**Englund et al., 2005**). In embryonic mouse neocortex, Tbr2 is not only expressed in the predominant type of BP, the basal intermediate progenitors (bIPs) which are known to be neurogenic (**Haubensak et al., 2004; Miyata et al., 2004; Noctor et al., 2004**), but also (in contrast to an earlier report (**Wang et al., 2011**)) in the vast majority of mitotic bRG (**Florio et al., 2015**), which exhibit a low proliferative capacity (**Wang et al., 2011**). In contrast, human bRG, which exhibit a high proliferative capacity (**Hansen et al., 2010; LaMonica et al., 2013**), largely lack Tbr2 expression (**Fietz et al., 2010; Hansen et al., 2010**). Extrapolating from these data on mouse and human BPs to the bRG in embryonic ferret neocortex, many of which express Tbr2 (**Reillo et al., 2011**), it appears justified to assume that a portion of the latter bRG may be neurogenic and exhibit a reduced proliferative capacity. Consistent with this assumption and with the effects of ARHGAP11B expression on neural progenitors in the developing ferret neocortex described so far, we observed, upon expression of ARHGAP11B for 7 days, a decrease in the proportion of Tbr2+ FP+ progenitors in all GZs, which was statistically significant for the VZ (**Figure 2D,E**).

In order to potentially obtain further cues as to the proliferative capacity of the ARHGAP11B-increased bRG in the developing ferret neocortex, we focused our attention on progenitor cells that (i) exhibited a radial morphology, (ii) expressed Sox2, but (iii) lacked Tbr2 expression (**Figure 2F**). Upon ARHGAP11B expression, we observed, in the sum of the GZs, a 20% increase in the proportion of radial Sox2+ cells that were Tbr2- (**Figure 2G**). This was largely due to an increase in the proportion of these cells in the OSVZ (**Figure 2H**), where more than 90% were Tbr2-. Considering that the ISVZ is the GZ with the highest amount of Tbr2+ BPs (**Figure 2A**), we examined the relative proportions of Sox2+ Tbr2- and Sox2+ Tbr2+ BPs in the ISVZ and did not observe any significant difference in these proportions between control and ARHGAP11B expression (**Figure 2—figure supplement 1**).

These findings are consistent with the notion that the ARHGAP11B-increased radial Sox2+ Tbr2- cells in the OSVZ are bRG. Studies in fetal human neocortex have established that such cells in the OSVZ are highly proliferative (**Hansen et al., 2010** and **LaMonica et al., 2013**; for reviews see **Florio and Huttner, 2014** and **Lui et al., 2011**). Hence, our finding that expression of ARHGAP11B in developing ferret neocortex results in a marked increase in the proportion of these cells suggests that this human-specific gene is sufficient to promote, in a gyrencephalic carnivore, the generation of bRG with putatively increased proliferative capacity.

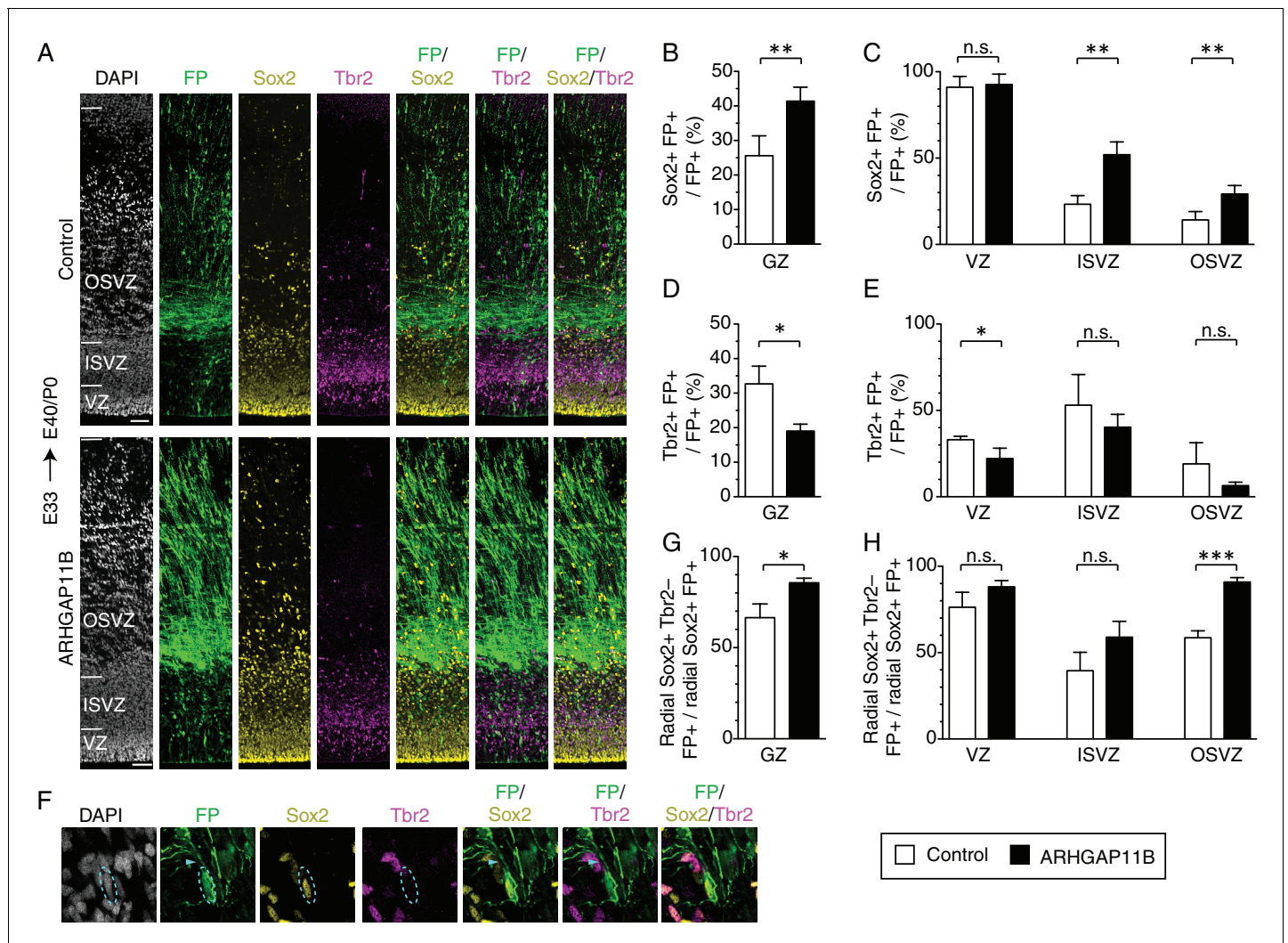


Figure 2. ARHGAP11B increases the proportion of Sox2-positive bRG that are Tbr2-negative. Ferret E33 neocortex was electroporated *in utero* with a plasmid encoding FP together with either a plasmid encoding ARHGAP11B or empty vector (Control), followed by triple immunofluorescence for FP (green), Sox2 (yellow) and Tbr2 (magenta), combined with DAPI staining (white), at E40/P0. (A) Overview of the electroporated areas (single optical sections). Scale bars, 50 μ m. (B, C) Percentage of FP+ cells in the germinal zones (B, GZ) and in the VZ (C, left), ISVZ (C, center) and OSVZ (C, right) that are Sox2+ upon control (white) and ARHGAP11B (black) electroporations. (D, E) Percentage of FP+ cells in the germinal zones (D, GZ) and in the VZ (E, left), ISVZ (E, center) and OSVZ (E, right) that are Tbr2+ upon control (white) and ARHGAP11B (black) electroporations. (F) Proliferative bRG (Sox2 + Tbr2- cell in the SVZ exhibiting radial morphology, single optical sections). Triple immunofluorescence for FP (green), Sox2 (yellow) and Tbr2 (magenta), combined with DAPI staining (white), upon electroporation of the plasmid encoding FP together with the plasmid encoding ARHGAP11B. Dashed lines, cell body; arrowheads, radial process. Images are oriented with the apical side facing down and are 25 μ m wide. (G, H) Percentage of Sox2+ FP+ cells exhibiting radial morphology in the germinal zones (G, GZ) and in the VZ (H, left), ISVZ (H, center) and OSVZ (H, right) that are Tbr2- upon control (white) and ARHGAP11B (black) electroporations. (B–E, G, H) Data are the mean of 4 experiments. Error bars indicate SD; ***, $p < 0.001$; **, $p < 0.01$; *, $p < 0.05$; n.s., not statistically significant; Student’s t-test.

DOI: <https://doi.org/10.7554/eLife.41241.006>

The following figure supplement is available for figure 2:

Figure supplement 1. ARHGAP11B expression does not affect the proportion of Sox2+ Tbr2+ vs. Sox2+ Tbr2- cells in the ISVZ.

DOI: <https://doi.org/10.7554/eLife.41241.007>

ARHGAP11B expression in developing ferret neocortex results in an extended neurogenic period

We investigated the potential consequences of the ARHGAP11B-elicited increase in the abundance of BPs, notably of Sox2+ Tbr2- bRG, for neurogenesis in the developing ferret neocortex. To this

end, we immunostained E40/P0 ferret neocortex for Tbr1, a transcription factor which is a marker of deep-layer neurons (Kolk et al., 2006) (Figure 3—figure supplement 1A), and for Satb2, a transcriptional regulator which is expressed in neurons that establish callosal projections and that are highly enriched in the upper layers of the cortical plate (CP) (Alcamo et al., 2008; Britanova et al., 2008) (Figure 3A). The vast majority (>90%) of the FP+ neurons in the CP of both control and ARHGAP11B-expressing ferret neocortex were found to be Satb2+ (Figure 3—figure supplement 1B). This high percentage is consistent with our experimental approach in which we targeted the embryonic ferret neural progenitors by *in utero* electroporation at E33, that is the time when the generation of the upper-layer neurons starts (Jackson et al., 1989; Martínez-Martínez et al., 2016).

Analysis of the distribution of Satb2+ FP+ neurons at E40/P0 between the CP on the one hand side, and the GZs plus the intermediate zone (IZ) on the other hand side, revealed that around 60% of the neurons had reached the CP in both control and ARHGAP11B-expressing ferret neocortex (Figure 3B left). We next examined electroporated ferret neocortex at P10 (Figure 3—figure supplement 2; analysis confined to gyri), which is the stage when neuron production is completed and neuron migration is terminating in the motor and somatosensory areas (Jackson et al., 1989; Smart and McSherry, 1986a; Smart and McSherry, 1986b). Consistent with this, our analysis of the control brains revealed that more than 90% of the Satb2+ FP+ neurons had reached the CP (Figure 3B middle). In contrast, only 70% of the Satb2+ FP+ neurons were found in the CP of the ARHGAP11B-expressing neocortex (Figure 3B middle). However, at P16, nearly all Satb2+ FP+ neurons were found in the CP in both control and ARHGAP11B-expressing neocortex (Figure 3B right; again, analysis confined to gyri). These data suggested that upon ARHGAP11B expression, either neurons migrate more slowly to the CP, or the neurogenic period is extended.

To explore the latter scenario, we injected EdU into P5 ferret kits (i.e. 12 days after electroporation), which is the stage when neuronal progenitors undergo their very last neuron-generating cell divisions in the motor and somatosensory areas of the neocortex (Jackson et al., 1989; Smart and McSherry, 1986a; Smart and McSherry, 1986b). Analysis 11 days after EdU injection, at P16 (Figure 3C), revealed a 4-fold increase in the proportion of FP+ cells that were EdU+, in neocortical gyri of ARHGAP11B-expressing kits compared to control (Figure 3D). This was consistent with a prolonged, and hence increased, production of cells in ARHGAP11B-expressing kits, which in turn would be in line with the above described finding that ARHGAP11B increases the abundance of proliferative bRG. Importantly, among the EdU+ FP+ cells of the ARHGAP11B-expressing neocortex, 20% were Satb2+ neurons (Figure 3C' and E). In contrast, we did not detect a single Satb2+ EdU+ FP+ neuron in any of the control neocortices (Figure 3E). Collectively, these data indicate that neurogenesis in ARHGAP11B-expressing ferret neocortex continues longer than in control neocortex.

ARHGAP11B expression in developing ferret neocortex results in a greater abundance of upper-layer neurons

In light of the extension of the neurogenic period upon ARHGAP11B expression, we examined a potential increase in the abundance of the last-born neurons, that is, the upper-layer neurons. To this end, we first performed Nissl staining of the P16 ferret neocortex to visualize all neurons and the various layers of the CP, and immunostaining for Satb2, which is expressed in the majority of upper-layer neurons (Alcamo et al., 2008; Britanova et al., 2008; Lodato and Arlotta, 2015) (Figure 4A). These analyses, carried out on gyri, revealed (i) an increase in the abundance of FP+ cells in the CP (Figure 4—figure supplement 1A), and (ii) an alteration in the distribution of the FP+ cells between layers II-VI of the CP, with a greater proportion of cells in layers II-IV (Figure 4—figure supplement 1B), in the ARHGAP11B-expressing neocortex compared to control. A similar abundance increase (Figure 4—figure supplement 1C) and altered distribution (Figure 4B) were observed for Satb2+ FP+ neurons. Furthermore, the proportion of FP+ cells in the CP that were Satb2+ neurons was increased upon ARHGAP11B expression (Figure 4C).

We sought to corroborate these data by immunostaining the P16 ferret neocortex for Brn2 (Pou3f2, Figure 4—figure supplement 2A), a transcription factor considered to be a marker of layer II and III neurons (Dominguez et al., 2013; McEvilly et al., 2002; Sugitani et al., 2002). Quantification of Brn2+ FP+ cells in layers II and III of gyri revealed a marked increase in the abundance of these cells (Figure 4—figure supplement 2B) and in the proportion of FP+ cells that were Brn2+ neurons (Figure 4D), in ARHGAP11B-expressing kits compared to control. Of note, the effects of

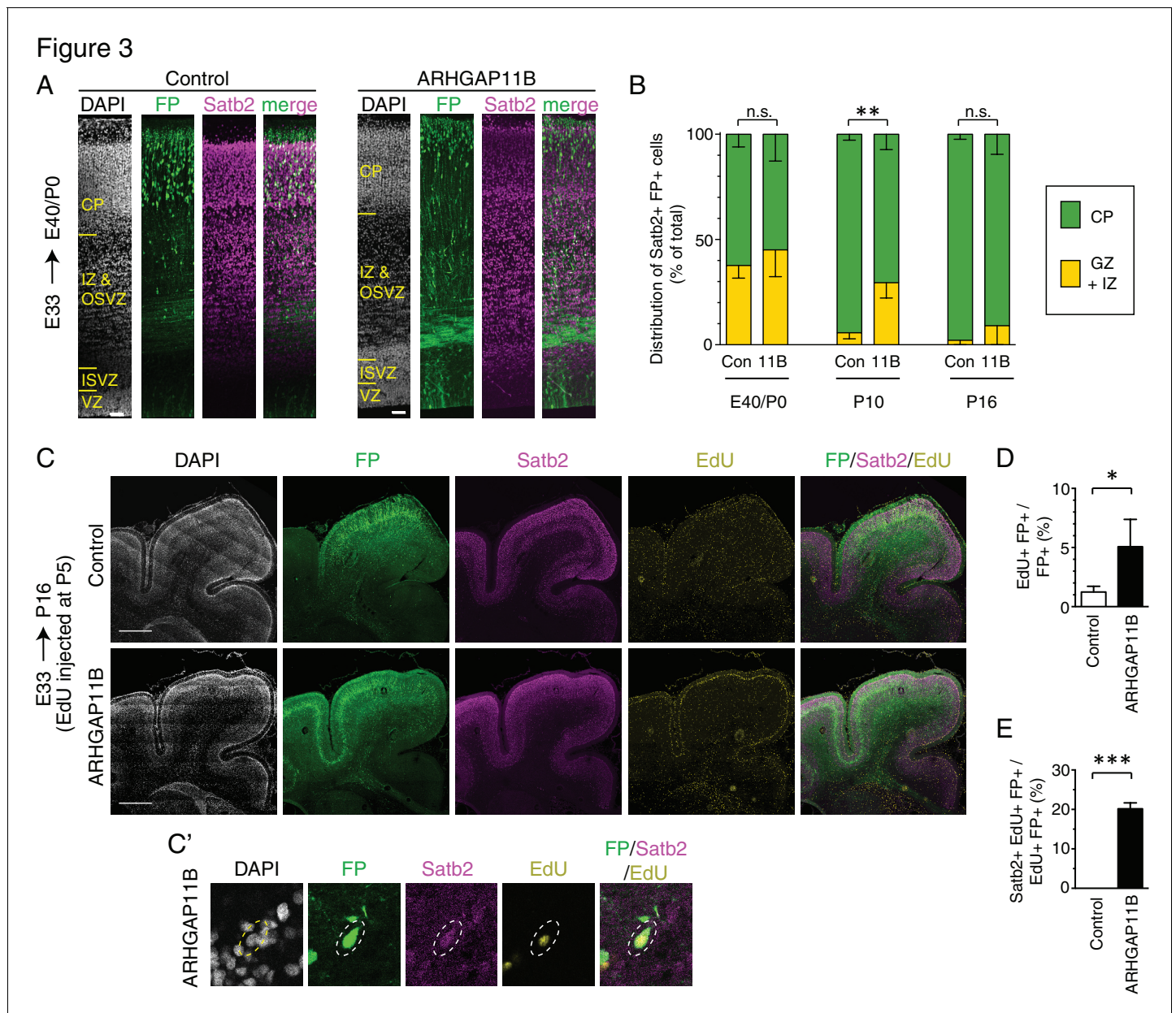


Figure 3. ARHGAP11B expression in developing ferret neocortex results in an extended neurogenic period. Ferret E33 neocortex was electroporated *in utero* with a plasmid encoding FP, together with either a plasmid encoding ARHGAP11B or empty vector (Control), followed by analysis at E40/P0 (A, B left), P10 (B center) and P16 (B right, C–E). (A) Double immunofluorescence for FP (green) and Satb2 (magenta), combined with DAPI staining (white), of the E40/P0 ferret neocortex. The immunofluorescence of the same cryosection for Tbr1 is shown in **Figure 3—figure supplement 1A**. Images are single optical sections. Scale bars, 50 μ m. (B) Distribution of Satb2+ FP+ neurons at E40/P0 (left), P10 (center) and P16 (right), between the cortical plate (CP, green) and germinal zones plus intermediate zone (GZ + IZ, yellow), upon control (Con, left) and ARHGAP11B (11B, right) electroporations. Data are the mean of 3 (P0 and P10) or 4 (P16) experiments. Error bars indicate SD; **, $p < 0.01$; n.s., not statistically significant; two-way ANOVA with Bonferroni post-hoc tests (P10, Control CP vs. ARHGAP11B CP, $p = 0.0015$). (C) Triple (immuno)fluorescence for FP (green), Satb2 (magenta) and EdU (yellow), combined with DAPI staining (white), of the P16 ferret neocortex, upon EdU injection at P5. Images are single optical sections. Scale bars, 1 mm. (C') Higher magnification of a FP+ Satb2+ EdU+ neuron upon electroporation of the plasmid encoding FP together with the plasmid encoding ARHGAP11B. Dashed lines, cell body. Images (single optical sections) are oriented with the apical side facing down and are 50 μ m wide. (D) Percentage of FP+ cells that are EdU+ upon control (white) and ARHGAP11B (black) electroporations. (E) Percentage of EdU+ FP+ cells that are Satb2+ upon control (white) and ARHGAP11B (black) electroporations. (D, E) Data are the mean of 3 experiments. Error bars indicate SD; ***, $p < 0.001$; *, $p < 0.05$; Student's t-test.

DOI: <https://doi.org/10.7554/eLife.41241.008>

The following figure supplements are available for figure 3:

Figure 3 continued on next page

Figure 3 continued

Figure supplement 1. Almost all neurons generated from ARHGAP11B-expressing progenitors are Satb2+.

DOI: <https://doi.org/10.7554/eLife.41241.009>

Figure supplement 2. FP and Satb2 immunostaining patterns of control and ARHGAP11B-expressing developing ferret neocortex at P10.

DOI: <https://doi.org/10.7554/eLife.41241.010>

ARHGAP11B expression on the Brn2+ neurons were of a greater degree than those on the Satb2+ neurons (compare **Figure 4—figure supplement 2B** with **Figure 4—figure supplement 1C**; **Figure 4**, panel D with panel C), in line with the notion that Brn2 exhibits a greater specificity for layer II and III neurons than Satb2 (*Dominguez et al., 2013*; *Sugitani et al., 2002*). Taken together, our data indicate that the extension of the neurogenic period upon ARHGAP11B expression in the developing ferret neocortex is accompanied by an increase in the abundance of layer II and III neurons.

ARHGAP11B expression in developing ferret neocortex leads to its radial and tangential expansion

Finally, we explored whether the ARHGAP11B-elicited increase in the abundance of BPs, notably of proliferative bRG, resulting in an extended neurogenic period and in an increased abundance of upper-layer neurons, had any consequences for the size and morphology of the ferret neocortex. To this end, we analyzed the neocortex at P16 (**Figure 4—figure supplement 3A–C**), the developmental stage when cortical folds have already formed in the ferret (*Barnette et al., 2009*; *Fernández et al., 2016*; *Matsumoto et al., 2017*; *Sawada and Watanabe, 2012*; *Shinmyo et al., 2017*), and quantified a set of morphological parameters (**Figure 4—figure supplement 3D**), each on two coronal sections located slightly rostrally (**Figure 4—figure supplement 3B and C**, position 1) and slightly caudally (**Figure 4—figure supplement 3B and D**, position 2), respectively, to a middle position along the rostro-caudal axis. This revealed no significant differences between control and ARHGAP11B-expressing kits with regard to brain mass (**Figure 4—figure supplement 3E**) and gross neocortex morphology, including the gyrification index of the electroporated area (referred to as local GI), the size of the posterior sigmoid gyrus, lateral gyrus and coronal gyrus, and the depth and thickness of the cruciate sulcus, suprasylvian sulcus and lateral sulcus (**Figure 4—figure supplement 3F–I**; for the gyri and sulci positions, see **Figure 4—figure supplement 3B–D**).

However, we did detect an increase, upon ARHGAP11B expression, in the thickness of the three gyri analyzed (**Figure 4E**). We therefore investigated the underlying cause of this thickness increase and, considering the increased abundance of upper-layer neurons upon ARHGAP11B expression (**Figure 4—figure supplement 1C**, **Figure 4—figure supplement 2B**), measured the thickness of CP layers II–IV in the gyri of control and ARHGAP11B-expressing ferret neocortex at P16. This revealed a 100 μm increase in the thickness of these upper layers in ARHGAP11B-expressing neocortex compared to control (**Figure 4F**, note also the thicker layer II in **Figure 4A** and another example in **Figure 4—figure supplement 5G**). Hence, ARHGAP11B is sufficient to promote neocortex expansion in ferret in the radial dimension.

We then explored whether ARHGAP11B would also be able to promote neocortex expansion in ferret in the tangential dimension. Here, we exploited the previous findings that during the first week of the ferret postnatal neocortex development, migrating neurons change their migration mode from radial to tangential, which results in an increased lateral dispersion of the late-born neurons (*Gertz and Kriegstein, 2015*; *Reillo et al., 2011*; *Smart and McSherry, 1986a*; *Smart and McSherry, 1986b*). In line with this, the abundance of FP+ cells per 200 μm -wide field of cortical wall decreased about 3-fold from E40/P0 to P16 (**Figure 4—figure supplement 4A**). Yet, the increase in FP+ cells per field of cortical wall due to ARHGAP11B expression was not only observed at P16, confirming the above described analysis of FP+ cell numbers in the CP (**Figure 4—figure supplement 1A**), but was already detected at E40/P0 (**Figure 4—figure supplement 4A**). The decrease in FP+ cell abundance per 200 μm -wide field of cortical wall from E40/P0 to P16 (**Figure 4—figure supplement 4A**) was not accompanied by an increase in cell death (**Figure 4—figure supplement 4B–G**). Rather, this decrease reflected an increase in the lateral spread of the progeny of the targeted cells, as evidenced by the ARHGAP11B-elicited increase in the lateral length of the area harbouring FP+ cells that was observed at P16 (**Figure 4G**, **Figure 4—figure supplement 5A**

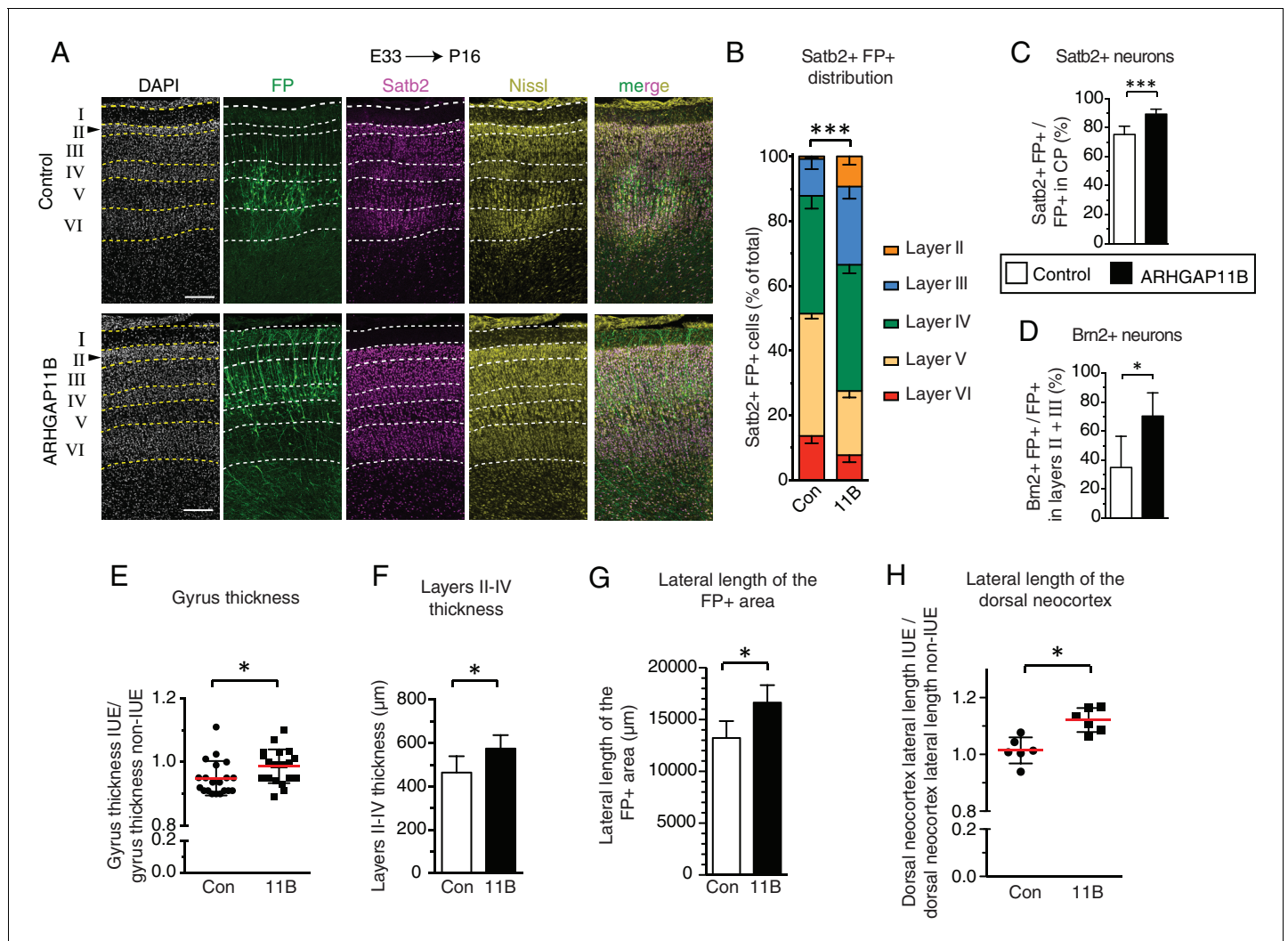


Figure 4. ARHGAP11B expression results in a greater abundance of upper-layer neurons and expansion of the developing ferret neocortex. Ferret E33 neocortex was electroporated *in utero* with a plasmid encoding FP, together with either a plasmid encoding ARHGAP11B or empty vector (Control), followed by analysis at P16. (A) Double immunofluorescence for FP (green) and Satb2 (magenta), combined with DAPI (white) and Nissl (yellow) staining, of the CP (single optical sections). Neuronal layers are marked on the left. Arrowheads, increased thickness of layer II upon ARHGAP11B expression. Scale bars, 200 µm. (B) Distribution of Satb2+ FP+ neurons between the neuronal layers upon control (Con, left) and ARHGAP11B (11B, right) electroporations. Data are the mean of 6 experiments. Error bars indicate SD; ***, $p < 0.001$; two-way ANOVA with Bonferroni post-hoc tests (Layer V, Control vs. ARHGAP11B, $p < 0.0001$; Layer III, Control vs. ARHGAP11B, $p = 0.0073$) (C) Percentage of FP+ cells in the CP that are Satb2+, upon control (white) and ARHGAP11B (black) electroporations. Data are the mean of 6 experiments. Error bars indicate SD; ***, $p < 0.001$; Student's t-test. (D) Percentage of FP+ cells in layers II + III that are Brn2+, upon control (white) and ARHGAP11B (black) electroporations. Data are the mean of 5 experiments. Error bars indicate SD; *, $p < 0.05$; Student's t-test. (E) Quantification of the gyrus thickness of control (Con) and ARHGAP11B-expressing (11B) ferret neocortex. Measurements were performed as described in **Figure 4—figure supplement 3**. All data are expressed as ratio between electroporated hemisphere (IUE) and non-electroporated contralateral hemisphere (non-IUE). Data are the mean (red lines) of 20 gyri per condition from six neocortices per condition. Error bars indicate SD; *, $p < 0.05$; Student's t-test. (F) Quantification of layers II-IV thickness, upon control (Con, white) and ARHGAP11B (11B, black) electroporations. Data are the mean of 6 experiments. Error bars indicate SD; *, $p < 0.05$; Student's t-test. (G) Quantification of the lateral length of the entire areas harbouring FP+ cells, measured as depicted in **Figure 4—figure supplement 5A** top, upon control (Con, white) and ARHGAP11B (11B, black) electroporations. Data are the mean of 6 experiments. Error bars indicate SD; **, $p < 0.01$; Student's t-test. (H) Quantification of the lateral length of the dorsal neocortex, measured as depicted in **Figure 4—figure supplement 5A** bottom, upon control (Con) and ARHGAP11B (11B) electroporations. All data are expressed as ratio between electroporated hemisphere (IUE) and non-electroporated contralateral hemisphere (non-IUE). Data are the mean of 6 experiments. Error bars indicate SD; *, $p < 0.05$; Student's t-test.

DOI: <https://doi.org/10.7554/eLife.41241.011>

The following figure supplements are available for figure 4:

Figure supplement 1. ARHGAP11B expression results in a greater abundance of FP+ cells and FP+ Satb2+ neurons in the CP.

Figure 4 continued on next page

Figure 4 continued

DOI: <https://doi.org/10.7554/eLife.41241.012>

Figure supplement 2. ARHGAP11B expression results in a greater abundance of FP+ Brn2+ neurons in cortical layers II and III.

DOI: <https://doi.org/10.7554/eLife.41241.013>

Figure supplement 3. ARHGAP11B expression in developing ferret neocortex does not increase neocortical folding.

DOI: <https://doi.org/10.7554/eLife.41241.014>

Figure supplement 4. ARHGAP11B expression in developing ferret neocortex does not lead to increased cell death.

DOI: <https://doi.org/10.7554/eLife.41241.015>

Figure supplement 5. ARHGAP11B expression in developing ferret neocortex leads to its tangential expansion and an increase in cell density.

DOI: <https://doi.org/10.7554/eLife.41241.016>

Figure supplement 6. ARHGAP11B induces the appearance of astrocytes from the targeted progenitors in the developing ferret neocortex.

DOI: <https://doi.org/10.7554/eLife.41241.017>

top, B). Of note, the increase in the lateral spread of FP+ cells persisted along the rostral-caudal axis of the FP+ region of the neocortex (**Figure 4—figure supplement 5C**) and did not reflect a difference in the electroporation efficiency, as the lateral length of the FP+ area on both the basal and apical side was not different between control and ARHGAP11B-expressing E40/P0 ferret neocortex (**Figure 4—figure supplement 5D,E**).

Importantly, the total lateral length of the dorsal neocortex was also increased upon ARHGAP11B expression (**Figure 4H**, **Figure 4—figure supplement 5A** bottom). This increase was observed at different positions along the rostral-caudal axis (**Figure 4—figure supplement 5F**). These data further imply that the increase in the lateral spread (**Figure 4G**, **Figure 4—figure supplement 5A** top, B) did not occur at the expense of the other, FP-, areas. We conclude that ARHGAP11B is sufficient to promote neocortex expansion in ferret also in the tangential dimension.

Given that the ARHGAP11B-elicited increase in the lateral length of the FP+ area ($\approx 25\%$, **Figure 4G**) was greater than the ARHGAP11B-elicited tangential expansion ($\approx 10\%$, **Figure 4H**), we explored whether this discrepancy could be resolved by ARHGAP11B expression increasing cell density, specifically in the upper layers of the CP where most of the ARHGAP11B-increased neurons resided. Indeed, our analysis revealed an increase in total cell density (revealed by DAPI staining) (**Figure 4—figure supplement 5G,H**) and in neuronal density (revealed by Satb2 immunostaining, **Figure 4—figure supplement 5G,I**) in layers III and IV at P16, but not in layer II, which in general exhibited the highest cell density. Taken together, these data indicate that the ARHGAP11B-induced increase in BP pool size led to an increase in upper-layer neurons that in turn resulted in (i) a thickening of the upper layers, (ii) a higher cell density in those upper layers that were able to accommodate additional neurons, (iii) a greater lateral spread of upper-layer neurons, and (iv) consequently, a greater lateral length of the dorsal neocortex.

ARHGAP11B induces the appearance of astrocytes from the targeted progenitors in the developing ferret neocortex

Neocortex expansion involves not only an increase in the number of neurons, but also of glial cells. Although we on purpose performed *in utero* electroporation of the ferret neocortex at E33 in order to target OSVZ progenitors generating upper-layer neurons (**Jackson et al., 1989**; **Martínez-Martínez et al., 2016**), and therefore would expect only a small proportion of the FP+ cells to be glial cells, we nonetheless examined the possible occurrence of GFAP+ and S100 β + cells (as indicators of an astrocytic lineage (**Reillo et al., 2011**; **Voigt, 1989**)) and of Olig2+ cells (as an indicator of an oligodendrocytic lineage (**Mo and Zecevic, 2009**; **Voigt, 1989**)) among the FP+ progeny of the targeted cells. An additional reason to examine astrocytes was that radial glial progenitor cells at later stages of human, monkey and ferret neocortex development are known to differentiate into astrocytic progenitors which then give rise to post-mitotic astrocytic cells (**Rakic, 1978**; **Rakic, 2003b**; **Reillo et al., 2011**; **Voigt, 1989**).

Upon immunostaining of the P16 ferret neocortex for GFAP (**Figure 4—figure supplement 5A,B**) and Olig2 (**Figure 4—figure supplement 5E**), no FP+ cells in the CP of control neocortex that were GFAP+ or Olig2+ could be detected. In contrast, while we still did not detect any Olig2+ FP+ cells in the CP of ARHGAP11B-expressing neocortex, about 3% of the CP FP+ cells were GFAP+ (**Figure 4—figure supplement 5C**). Given that ARHGAP11B expression increases the pool size of FP

+ cells (**Figure 4—figure supplement 1A**, **Figure 4—figure supplement 4A**), this translates into an ARHGAP11B-induced appearance of GFAP+ FP+ cells in the CP. All of these GFAP+ FP+ cells were Ki67– (data not shown) and hence post-mitotic astrocytes. To corroborate these data, we performed immunostaining of the P16 ferret neocortex for another astrocyte marker, S100 β (**Figure 4—figure supplement 5D**) (**López-Hidalgo et al., 2016**), and readily identified FP+ S100 β + astrocytes upon ARHGAP11B expression. These data are consistent with at least two scenarios related to the increased abundance of proliferative bRG upon ARHGAP11B expression. Either this increase results not only in an extension of the neurogenic period but also in the initiation of astrogenesis. Or the greater bRG pool size gives rise to a detectable level of astrocytic cells once the bRG differentiate along the astrocytic lineage (**Rakic, 2003b; Reillo et al., 2011; Voigt, 1989**).

Discussion

We have shown that expression of a single human-specific gene, *ARHGAP11B*, which has been implicated in the evolutionary expansion of the human neocortex (**Florio et al., 2015; Florio et al., 2016**), is sufficient to elicit features in the developing ferret neocortex that are characteristically associated with a further expanded neocortex such as human. These features include (i) an increase in the pool size of proliferative BPs, notably proliferative bRG; (ii) a lengthening of the neurogenic period; (iii) an increased generation of neurons, in particular of upper-layer neurons; and (iv) an increase in the size of the CP that harbours these additional neurons, reflected by a greater thickness of its upper layers and a larger lateral length of the dorsal neocortex.

Increase in proliferative bRG

The present effects of *ARHGAP11B* on BPs in developing ferret neocortex are substantially greater than, and significantly different from, those previously observed upon transient *ARHGAP11B* expression in embryonic mouse neocortex (**Florio et al., 2015**), with regard to BP quantity and quality. As to quantity, in embryonic mouse neocortex, *ARHGAP11B* expression resulted in a doubling and tripling of the pool size of total BPs and BPs in mitosis, respectively (**Florio et al., 2015**), whereas in embryonic ferret neocortex, *ARHGAP11B* expression led to nearly tripling and quintupling of the pool size of total BPs and BPs in mitosis (notably mitotic bRG), respectively (for a data summary, see **Supplementary file 1**). The greater effect of *ARHGAP11B* expression on mitotic BP abundance than total BP abundance, in both embryonic mouse and ferret neocortex, indicates that *ARHGAP11B* expression increases the proportion of the total duration of the BP cell cycle that is used for M-phase. This in turn would be consistent with *ARHGAP11B* promoting, in embryonic ferret neocortex, the proliferative rather than neurogenic mode of bRG division. This notion would be in line with the previous findings that both, cortical progenitors in embryonic mouse neocortex (**Arai et al., 2011**) and radial glial progenitors in postnatal ferret neocortex (**Turrero García et al., 2016**), which are not yet committed to neurogenesis spend a greater proportion of their total cell cycle in M-phase than those committed to neurogenesis.

Regarding the regulation of cell cycle length, it appears worthwhile to consider the present increase in BP abundance upon *ARHGAP11B* expression in developing ferret neocortex in the context of previous findings showing that shortening the duration of the G1 phase in progenitors of both mouse (**Lange et al., 2009; Pilaz et al., 2009**) and ferret (**Nonaka-Kinoshita et al., 2013**) developing neocortex results in increased BP proliferation and neocortex expansion. Furthermore, manipulation of cyclins or cdk/cyclin complexes was shown to lead to an increase in upper layer and callosal projection neurons (**Lange et al., 2009; Nonaka-Kinoshita et al., 2013; Pilaz et al., 2009**), which again is consistent with the phenotypes observed in the present study upon expression of *ARHGAP11B* in the developing ferret neocortex.

As to BP quality, mouse bRG have been shown to undergo mostly neurogenic cell divisions and to display a limited proliferative capacity (**Shitamukai et al., 2011; Wang et al., 2011; Wong et al., 2015**). In contrast, human bRG are known to be highly proliferative, which is thought to be one of the key factors contributing to the evolutionary expansion of the human neocortex (**Fietz et al., 2010; Florio and Huttner, 2014; Hansen et al., 2010; Lui et al., 2011**). The proliferative capacity of bRG in other mammalian species that have been studied appears to follow the general rule that highly proliferative bRG are more often found in species with an expanded neocortex (**Betizeau et al., 2013; Reillo et al., 2011**). Hence, the *ARHGAP11B*-promoted increase in the

number of proliferative (Sox2+ Tbr2-) bRG in the developing ferret neocortex fulfills a key requirement for further neocortex expansion.

In this context, it should be emphasized that those of the human-specific genes (*Dennis and Eichler, 2016*) that have been shown to be preferentially expressed in cortical progenitor cells (*Florio et al., 2018*) and that have been ectopically expressed in embryonic mouse neocortex, that is *ARHGAP11B* (*Florio et al., 2015*) and *NOTCH2NL* (*Fiddes et al., 2018; Florio et al., 2018; Suzuki et al., 2018*), show an increase in BP proliferation that mostly involves basal intermediate progenitors. To the best of our knowledge, our study provides first evidence of a human-specific gene increasing the number of proliferative bRG in a gyrencephalic neocortex. As bRG are considered to be instrumental for the evolutionary expansion of neocortex, this suggests that the ferret likely is a model system superior to mouse for studying the role of human-specific genes in neocortex development.

Increase in upper-layer neurons

An increase in the upper layers is a fundamental characteristic of neocortex expansion (*Fame et al., 2011; Hutsler et al., 2005; Molnár et al., 2006; Tarabykin et al., 2001*). Layers II-IV are evolutionarily the most novel and mammalian-specific layers (*Molnár et al., 2006*). Layers II and III, in particular, underwent disproportional expansion during primate evolution. As the layers II-III neurons are the last-born neurons, an increase in the length of the neurogenic period might result in an increase in the number of late-born neurons. In fact, it has been proposed that the length of the neurogenic period may be a contributing factor in explaining the evolutionary increase in neocortex size and neuron number between humans and other great apes (*Lewitus et al., 2014*). Consistent with this, we observed a prolonged generation of late-born neurons, increased thickness of layers II-IV, and a marked increase in Satb2+ (3.3-fold) and, in particular, Brn2+ (5.6-fold) neurons in the upper layers of the CP, upon *ARHGAP11B* expression (for a data summary, see *Supplementary file 1*). Thus, also with regard to the key product generated by cortical progenitor cells, that is the neurons, *ARHGAP11B* is sufficient to promote another feature in the developing ferret neocortex that would be consistent with further neocortex expansion.

In this context, Satb2+ neurons are of special interest, as Satb2 is essential for establishing callosal projections to the contralateral hemisphere (*Alcamo et al., 2008; Britanova et al., 2008*). Callosal projection neurons are considered to play a key role in the high-level associative connectivity, thus contributing significantly to human cognitive abilities, with their impairment causing cognition-related pathologies (*Fame et al., 2011*). Given that the evolutionary increase in neocortex size is accompanied by an increase in callosal projection neurons, our data show that *ARHGAP11B* elicits yet another, specific feature in the developing ferret neocortex associated with further neocortex expansion.

Neocortex expansion vs. increased thickness and lateral area

A hallmark of neocortex expansion is neocortical folding (*Borrell, 2018; Borrell and Götz, 2014; Kroenke and Bayly, 2018*). Transient expression of *ARHGAP11B* in the embryonic mouse neocortex induced cortical folding in about half of the cases in this normally lissencephalic rodent (*Florio et al., 2015*). However, expression of *ARHGAP11B* in the developing ferret neocortex did not significantly increase the GI, gyrus size, or sulcus depth and thickness in this gyrencephalic carnivore. The major morphological signs of neocortical expansion upon *ARHGAP11B* expression in developing ferret neocortex that we could detect were (i) an increased gyrus thickness, which reflected the already discussed increase in upper-layer thickness due to the increase in upper-layer neurons, and (ii) a larger lateral area of the CP where these neurons were found. The latter phenotype resulted in a $\approx 10\%$ increase in the lateral length of the dorsal neocortex, which however did not appear to be sufficient to significantly increase the gyrus size or GI.

The reason why a 3–5-fold increase in upper-layer neurons (*Supplementary file 1*) resulted in more modest increases in upper-layer thickness and dorsal neocortex lateral length (24% and 10%, respectively) could be that either (i) the increase in the number of FP+ neurons occurred at the expense of FP- neurons, or (ii) that the FP+ neurons added themselves to the FP- neurons already existing in the control condition, thereby increasing neuronal cell density in the upper layers. Our results show that the latter scenario is the case, as we detected a significant increase in both the

total cell density and neuronal density in the upper cortical layers upon ARHGAP11B expression. Analysis of cortical neuron density as a function of cortical neuron number across carnivores has revealed that neuron density tends to decrease with increasing neuron number (*Herculano-Houzel et al., 2015; Jardim-Messeder et al., 2017; Lewitus et al., 2012*). This trend is much less prominent in primates, which in general exhibit a greater cortical neuron density per cortical neuron number than carnivores. Thus, the increase in upper-layer neuron density upon increasing upper-layer neuron number by the human-specific *ARHGAP11B* can be regarded as a form of ‘primatization’ of the ferret neocortex.

In this context, it is interesting to note that neocortical neuron density across carnivores shows a much greater range of variation than that across primates (*Herculano-Houzel et al., 2015; Lewitus et al., 2012*). We therefore hypothesize that the ferret neocortex is plastic enough to accommodate additional neurons, without having to increase neocortex size or folding. A corollary of this notion with regard to *ARHGAP11B* is that its primary function is to increase the proliferation and thus pool size of BPs, notably of bRG, which results in a lengthening of the neurogenic period and an increased generation of neurons, in particular of upper-layer neurons. In embryonic mouse neocortex, the *ARHGAP11B*-elicited increase in BPs could induce cortical folding as an indicator of neocortex expansion (*Florio et al., 2015*). In contrast, in the developing ferret neocortex studied here, the *ARHGAP11B*-elicited BP increase did not further increase the GI, although it did increase the neurogenic period and upper-layer neurons. This in turn resulted in a greater thickness of the upper layers, increased neuron density, and a larger lateral length of the dorsal neocortex. The difference between the phenotypes observed in mouse and ferret developing neocortex therefore appears to reflect how species in different mammalian orders tend to deal with an increase in cortical neuron number, rather than the primary function of *ARHGAP11B*.

Materials and methods

Key resources table

Reagent type (species) or resource	Designation	Source or reference	Identifiers	Additional information
Antibody	Goat polyclonal anti-Sox2	R + D Systems	AF2018, RRID:AB_355110	(1:200)
Antibody	Goat polyclonal anti-Sox2	Santa Cruz Biotechnology	sc-17320 RRID:AB_2286684	(1:200)
Antibody	Rabbit polyclonal anti-Tbr2	Abcam	ab23345, RRID:AB_778267	(1:250)
Antibody	Mouse monoclonal anti-PCNA	Millipore	CBL407, RRID:AB_93501	(1:200)
Antibody	Mouse monoclonal anti-PhVim	Abcam	ab22651, RRID:AB_447222	(1:200)
Antibody	Mouse monoclonal anti-Satb2	Abcam	ab51502, RRID:AB_882455	(1:200)
Antibody	Rabbit polyclonal anti-Tbr1	Abcam	ab31940, RRID:AB_2200219	(1:200)
Antibody	Rabbit polyclonal anti-Brn2	Proteintech	18998-1-AP, RRID:AB_10597389	(1:100)
Antibody	Rabbit polyclonal anti-Olig2	Millipore	ab9610, RRID:AB_570666	(1:500)

Continued on next page

Continued

Reagent type (species) or resource	Designation	Source or reference	Identifiers	Additional information
Antibody	Rabbit polyclonal anti-GFAP	Dako	Z0334, RRID:AB_10013382	(1:1000)
Antibody	Rabbit polyclonal anti-S100 β	Abcam	ab868, RRID:AB_306716	(1:200)
Antibody	Rabbit polyclonal anti-active Caspase 3	Abcam	ab2302, RRID:AB_302962	(1:200)
Antibody	Mouse monoclonal anti-ARHG AP11B	MPI-CBG		(1:100)
Antibody	Rabbit polyclonal anti-Arhgap11A	Abcam	ab113261, RRID:AB_10866587	(1:500)
Antibody	Chicken polyclonal anti-GFP	Aves labs	GFP1020, RRID:AB_10000240	(1:1000)
Antibody	Goat polyclonal anti-GFP	MPI-CBG		(1:1000)
Antibody	Rat monoclonal anti-RFP	ChromoTek	5F8, RRID:AB_2336064	(1:500)
Antibody	Rabbit polyclonal anti-RFP	Rockland antibodies	600-401-379, RRID:AB_2209751	(1:1000)
Antibody	Goat polyclonal anti-Chicken Alexa Fluor 488	ThermoFisher Scientific	A11039, RRID:AB_142924	(1:500)
Antibody	Donkey polyclonal anti-Goat Alexa Fluor 488	ThermoFisher Scientific	A11055, RRID:AB_2534102	(1:500)
Antibody	Donkey polyclonal anti-Goat Alexa Fluor 555	ThermoFisher Scientific	A21432, RRID:AB_2535853	(1:500)
Antibody	Donkey polyclonal anti-Goat Alexa Fluor 647	ThermoFisher Scientific	A21447, RRID:AB_141844	(1:500)
Antibody	Donkey polyclonal anti-Rabbit Alexa Fluor 488	ThermoFisher Scientific	A21206, RRID:AB_141708	(1:500)
Antibody	Donkey polyclonal anti-Rabbit Alexa Fluor 555	ThermoFisher Scientific	A31572, RRID:AB_162543	(1:500)
Antibody	Donkey polyclonal anti-Rabbit Alexa Fluor 647	ThermoFisher Scientific	A-31573, RRID:AB_2536183	(1:500) or (1:1000)
Antibody	Donkey polyclonal anti-Mouse Alexa Fluor 488	ThermoFisher Scientific	A-21202, RRID:AB_141607	(1:500) or (1:1000)

Continued on next page

Continued

Reagent type (species) or resource	Designation	Source or reference	Identifiers	Additional information
Antibody	Donkey polyclonal anti-Mouse Alexa Fluor 555	ThermoFisher Scientific	A31570, RRID:AB_2536180	(1:500)
Antibody	Donkey polyclonal anti-Mouse Alexa Fluor 647	ThermoFisher Scientific	A31571, RRID:AB_162542	(1:500)
Antibody	Goat polyclonal anti-Rat Alexa Fluor 555	ThermoFisher Scientific	A21434, RRID:AB_141733	(1:500) or (1:1000)
Antibody	Goat polyclonal anti-Rabbit Cy2	Jackson Immuno research	# 111-225-144, RRID:AB_2338021	(1:500)
Antibody	Goat polyclonal anti-Mouse Cy3	Jackson Immuno research	#115-165-166, RRID:AB_2338692	(1:500)
Antibody	Goat polyclonal anti-Mouse Cy5	Jackson Immuno research	#115-175-166, RRID:AB_2338714	(1:500)
Commercial assay or kit	Maxi prep kit	Qiagen	Cat#12362	
Commercial assay or kit	RNeasy FFPE RNA isolation kit	Qiagen	Cat# 73504	
Commercial assay or kit	NeuroTrace™ 640/660 deep-red fluorescent Nissl stain	Molecular probes	Cat# N-21483, RRID:AB_2572212	
Commercial assay or kit	In Situ Cell Death Detection Kit, TMR red (TUNEL)	Sigma-Aldrich	12156792910	
Commercial assay or kit	Annexin V Cy5 reagent	Biovision	1013–200	
Commercial assay or kit	Click-iT EdU Alexa Fluor 647 Imaging Kit	Invitrogen	C10340	
Strain, strain background (<i>Mustela putorius furo</i>)	Ferret	Marshall Bioresources		
Strain, strain background (<i>Mustela putorius furo</i>)	Ferret	Euroferret		
Sequence-based reagent	Hprt1 FqHprt1_F TACGCTGAG GATTTGAAAAG	This paper		oligonucleotide
Sequence-based reagent	Hprt1 FqHprt1_R CCATTCCTT CATCAGTCTC	This paper		oligonucleotide
Sequence-based reagent	ARHGAP11B qARHGAP11B_1F CAGAAAAGA AGGGCGTGAC	This paper		oligonucleotide

Continued on next page

Continued

Reagent type (species) or resource	Designation	Source or reference	Identifiers	Additional information
Sequence-based reagent	ARHGAP11B qARHGAP11B_1R GGAGTAGCAC AGAGACCATCA	This paper		oligonucleotide
Sequence-based reagent	ARHGAP11B qARHGAP11B_2F TGAGAATAAGA TGGATAGCAGCA	This paper		oligonucleotide
Sequence-based reagent	ARHGAP11B qARHGAP11B_2R GGTACACGCC CTTCTTTTCTG	This paper		oligonucleotide
Recombinant DNA reagent	pCAGGS	(<i>Florio et al., 2015</i>)		
Recombinant DNA reagent	pCAGGS-ARHGAP11B	(<i>Florio et al., 2015</i>)		
Recombinant DNA reagent	pCAGGS-mCherry	(<i>Tavano et al., 2018</i>)		
Recombinant DNA reagent	pCAGGS-GFP	(<i>Fei et al., 2014</i>)		
Software, algorithm	Fiji/ImageJ	Fiji/Imagej	https://imagej.nih.gov/ij/	
Software, algorithm	Prism	GraphPad software		
Software, algorithm	ZEN	Carl Zeiss		

Experimental animals

All experimental procedures were conducted in agreement with the German Animal Welfare Legislation after approval by the Landesdirektion Sachsen (licences TVV 2/2015 and TVV 21/2017). Timed-pregnant ferrets (*Mustela putorius furo*) were obtained from Marshall BioResources (NY, USA) or Euroferret (Copenhagen, Denmark) and housed at the Biomedical Services Facility (BMS) of MPI-CBG. Observed mating date was set to E0. Animals were kept in standardized hygienic conditions with free access to food and water and with an 16 hr/8 hr light/dark cycle. All experiments were performed in the dorsolateral telencephalon of ferret embryos, at a medial position along the rostro-caudal axis, in the prospective motor and somatosensory cortex.

Plasmids

All plasmids used in this study were previously published (see the Key Resources table). All plasmids were extracted and purified using the EndoFree Plasmid Maxi kit (QIAGEN) following the manufacturer's instructions.

In utero electroporation of ferrets

In utero electroporation of ferrets was performed as originally established by Dr. Hiroshi Kawasaki with the modifications listed below (*Kawasaki et al., 2012*). Pregnant jills (with embryos at E33) were kept fasted for at least 3 hr before the surgery. They were first placed in the narcosis box with 4% isoflurane. When in deep anesthesia, the ferrets were placed on the operation table and attached to the narcosis mask with a constant 3% isoflurane flow. Subsequently, the ferrets were injected subcutaneously with analgesic (0.1 ml Metamizol, 50 mg/kg), antibiotic (0.13 ml Synulox, 20 mg/kg or 0.1 ml amoxicilin, 10 mg/kg) and glucose (10 ml 5% glucose solution). A drop of Dexpanthenol Ointment solution was placed on their eyes to prevent eye dehydration during the surgical procedure. The ferret bellies were then shaved, sterilized with iodide and surgically opened. The uterus was exposed and embryos were injected intraventricularly with a solution containing 0.1% Fast Green (Sigma) in sterile PBS, 2.5 µg/µl of either pCAGGS vector (control) or pCAGGS-

ARHGAP11B vector, in either case together with 1 µg/µl of pCAGGS vector encoding a fluorescent protein (pCAGGS-GFP or pCAGGS-mCherry). For embryonic studies where the position of the electroporated embryos in the uterus was known, the same fluorescent protein-encoding vector was co-electroporated together with either control or ARHGAP11B-expressing vectors. For postnatal studies, pCAGGS and pCAGGS-ARHGAP11B were co-electroporated with different fluorescent protein-encoding vectors to enable distinction of kits. For different experiments, these vectors were alternated. Electroporations were performed with six 50-msec pulses of 100 V at 1 s intervals. Following electroporation, uterus was placed back in the peritoneal cavity and the muscle layer with the peritoneum were sutured using a 4–0 suture. The skin was sutured intracutaneously using the same thickness of the suture. Animals were carefully monitored until they woke up and then underwent postoperative care for the following 3 days (2 x daily 10 mg/kg amoxicilin, 3 x daily 25 mg/kg Metamizol).

EdU labeling of ferret kits

For the neurogenic length experiments, a single pulse of EdU was injected intraperitoneally at P5, that is 13 days after *in utero* electroporations, and the animals were sacrificed 11 days later, at P16. The protocol for EdU injection was the same as the one previously published for ferret kits (Turrero García *et al.*, 2016).

Isolation of ferret brains

Ferret embryos were isolated at E37 and E40. Ferret kits were sacrificed at P0, P10 and P16. For the isolation of embryos, pregnant jills underwent the second surgery that followed the same pre-operative care, anesthesia and analgesia as the first surgery. The sutures from the first operation were carefully removed and the uterus was exposed. A caesarian section was made and embryos were removed from the uterus. Subsequently a complete hysterectomy was performed, after which the muscle layer with peritoneum and skin were sutured and the animal underwent the same post-operative care as after the first surgery. Embryonic brains were isolated and fixed at 4°C for 48 hr in 4% paraformaldehyde in 120 mM phosphate buffer pH 7.4.

For the postnatal time points, the kits were sacrificed by intraperitoneal injection of 4 mg/kg Xylazine +40 mg/kg Ketamin. When in deep anaesthesia, the kits were perfused intracardially with PBS, followed by perfusion with 4% paraformaldehyde in 120 mM phosphate buffer pH 7.4 at room temperature. Kit brains were then isolated and fixed for 48 hr in 4% paraformaldehyde in 120 mM phosphate buffer pH 7.4 at 4°C.

Ferret jills whose kits were used postnatally also underwent the second surgery with the hysterectomy. Upon this surgery, they underwent the same post-operative care as after the first surgery. All jills were kept at the BMS of the MPI-CBG for at least two weeks after the second surgery. Afterwards they were donated for adoption. No adult ferrets were sacrificed in this study.

Preparation of ferret brain slices

Upon fixation ferret brains were sectioned either on a vibratome or cryostat. Vibratome sections were 70 µm thick. Thickness of cryosections varied from 35 to 60 µm. Vibratome sections were either immunostained freshly prepared or conserved in cryoprotectant solution (30% sucrose, 30% ethylene glycol, 1% PVP40, 1.3 mM NaH₂PO₄, 3.9 mM Na₂HPO₄, 15 mM NaCl) and stored at –20°C for later use.

Gene expression analysis by RT-qPCR

For analysis of *ARHGAP11B* expression, total RNA was isolated from two to three cryosections per developmental stage, using the RNeasy FFPE RNA isolation kit (Qiagen) including DNase-treatment following the manufacturer's instructions. An additional DNase-treatment was performed on the isolated RNA using the DNA-free DNA Removal Kit (Life technologies). cDNA was synthesized using random hexamers and Superscript III Reverse Transcriptase (Life Technologies). qPCR was performed using the Light Cycler SYBR green Master mix (Roche) on a Light Cycler 96 (Roche). Gene expression data were normalized based on the housekeeping gene *Hprt1*. Primer sequences are provided in the Key Resources Table.

Immunofluorescence

Immunofluorescence was performed as previously described (Kalebic et al., 2016). Antigen retrieval (1 hr incubation with 10 mM citrate buffer pH 6.0 at 70°C in a water bath or oven) was performed for the following samples: all E37 samples, all E40/P0 samples, and vibratome sections of P10 and P16 samples which were used for immunostainings of the nuclear markers (Satb2, Brn2, Sox2, Olig2 and Ki67). When immunofluorescence for Tbr2 (E40/P0) was performed, a modified antigen retrieval protocol was used (1 hr incubation with 10 mM citrate buffer pH 6.0 supplemented with 0.05% Tween-20 at 80°C in a water bath). Antigen retrieval was followed by three washes with PBS.

All the immunostainings, except the one for ARHGAP11B, were done as follows. Samples were subjected to permeabilization for 30 min in 0.3% Triton X-100 in PBS at room temperature, followed by quenching for 30 min in 0.1 M glycine in PBS at room temperature. Blocking was performed in a blocking solution (0.2% gelatin, 300 mM NaCl, 0.3% Triton X-100 in PBS) for 30 min. Primary antibodies were incubated in the blocking solution for 48 hr at 4°C. Subsequently, the sections were washed three times in the blocking solution, incubated with secondary antibodies (1:500) and DAPI (Sigma) in the blocking solution for 1 hr at room temperature, and washed again three times in the blocking solution before being either used for Nissl post-staining or directly mounted on microscopy slides with Mowiol.

For the immunostaining for ARHGAP11B, permeabilization was performed for 1 hr in the 0.3% Triton X-100 solution at room temperature. Quenching was performed as for the other immunostainings. Blocking was done in 10% horse serum supplemented with 0.3% Triton X-100 (HS blocking solution) for 1 hr. Primary antibodies were incubated in the same solution for 24 hr, at 4°C. Subsequently, sections were washed five times in the HS blocking solution, incubated with the secondary antibodies (1:1000) and DAPI in the HS blocking solution for 1 hr at room temperature, washed five times in PBS and mounted on microscopy slides with Mowiol. ARHGAP11B antibody used in this study is a mouse monoclonal antibody raised against a recombinant full length ARHGAP11B. As the first 220 amino acids of ARHGAP11B are 89% identical to the first 220 amino acids of the ferret Arhgap11a, we showed by immunostaining that the antibody we used did not recognize the endogenous ferret Arhgap11a (Figure 1—figure supplement 1E).

Staining with the Nissl fluorescent stain, EdU detection, annexin V labeling, and TUNEL labeling were performed after the antibody stainings. NeuroTrace™ 640/660 deep-red fluorescent Nissl stain (Molecular probes) was used, following the manufacturer's instructions. EdU staining was performed using Click-iT EdU Alexa Fluor 647 Imaging kit (Invitrogen), following the manufacturer's instructions. Annexin V labeling was performed using the Annexin V-Cy5 bright fluorescence reagent (BioVision), following the manufacturer's instructions. TUNEL labeling was performed using the In situ cell death detection kit, TMR red (Sigma-Aldrich), following the manufacturer's instructions.

Image acquisition

Images of whole ferret brains (Figure 4—figure supplement 3A) were obtained as follows. Images were acquired using an iPhone 7 and taking a photography of the brain through a UV-protection filter mounted on a SZX 16 Olympus stereomicroscope, equipped with a fluorescence lamp.

Fluorescent images were acquired using a Zeiss LSM 880 upright single-photon point scanning confocal system. For the embryonic stages, images were taken as either 1 μm single optical sections with the 40x objective or 2 μm single optical sections with the 20x objective. For the postnatal stages, images were taken as either 2 μm single optical sections with the 20x objective or 7.2 μm single optical sections with the 10x objective. When the images were taken as tile scans, the stitching of the tiles was performed using the ZEN software. Subsequently, all images were analyzed and processed with ImageJ (<http://imagej.nih.gov/ij/>).

Quantifications

All cell counts were performed in standardized microscopic fields using Fiji, processed using Excel (Microsoft), and results were plotted using Prism (GraphPad Software). For each condition, data (typically at least three microscopic fields) from one experiment (see definition below) were pooled, and the mean of the indicated number of experiments was calculated. Whenever possible the quantifications were done blindly.

The definition of the morphological parameters is depicted graphically in the **Figure 4—figure supplement 3D**. All the morphological parameters except the lateral length of the dorsal neocortex were quantified at two positions (referred to as positions 1 and 2) in the somatosensory cortex, as defined in **Figure 4—figure supplement 3B**, for the following gyri and sulci: posterior sigmoid gyrus, coronal gyrus, lateral gyrus, cruciate sulcus, suprasylvian sulcus and lateral sulcus (**Sawada and Watanabe, 2012**). All the morphological parameters are presented as a ratio of the value of the electroporated hemisphere and the value of the contralateral hemisphere, as established previously (**Matsumoto et al., 2017**). Calculations were as follows.

Local Gyrfication Index (Local GI): $\frac{\text{The length of the inner contour}}{\text{The length of the outer contour}}$

Local gyrfication index is calculated as a ratio of the local GI of the electroporated area and the local GI of the equivalent area on the contralateral side. Gyrus size is calculated as a ratio of the size of an electroporated gyrus and the size of the equivalent gyrus of the contralateral side. Sulcus depth is calculated as a ratio of the length of the line connecting the outer contour and the bottom of a sulcus and the equivalent line on the contralateral side. Sulcus thickness is calculated as a ratio of the thickness measured from the ventricular surface to the bottom of an electroporated sulcus and the equivalent thickness on the contralateral side. Gyrus thickness is calculated as a ratio of the thickness measured from the ventricular surface to the top of an electroporated gyrus and the equivalent thickness on the contralateral side. The upper layers thickness was measured as distance between the top of layer II and bottom of layer IV.

Lateral length of the FP+ area was measured as the distance between the medial-most and the lateral-most FP+ cell on a coronal cross-section, following the inner contour of the neocortex. The lateral length of the dorsal neocortex was measured at three positions along the rostro-caudal axis (positions 1 and 2, and position 1.5 located between positions 1 and 2 (**Figure 4—figure supplement 5C** bottom)), and was defined as a distance between the cingulate gyrus and ectosylvian gyrus along the inner contour, as depicted in **Figure 4—figure supplement 5A** bottom.

Total cell density was measured as number of DAPI+ nuclei in 50 μm x 50 μm fields. Neuronal density was measured as number of Satb2+ nuclei in the 50 μm x 50 μm fields.

Statistical analysis

All statistics analyses were conducted using Prism (GraphPad Software). Sample sizes are reported in each figure legend, where the term 'one experiment' would refer to one embryo for analysis at E37 or E40, and to one kit for postnatal analysis. Total number of litters analyzed was as follows: E37, two litters; E40/P0, four litters; P10, two litters; P16, three litters. Embryos or kits from all litters were included in the statistical analyses. Tests used were Two-way ANOVA with Bonferroni posttest and Student's *t*-test. For each quantification, the statistical test and significance are indicated in the figure legend.

Acknowledgements

We are grateful to the Services and Facilities of the Max Planck Institute of Molecular Cell Biology and Genetics for the outstanding support provided, notably J Helppi and his team of the Biomedical services (BMS) for the excellent husbandry of ferrets, J Peychl and his team of the Light Microscopy Facility and P Keller and his team of the Antibody Facility. We would like to particularly thank Anke Münch-Wuttke for help with perfusion of ferret kits and Dr. Anna Pfeffer for exceptional veterinary support. NK was supported by an EMBO long-term fellowship (ALTF 861–2013). CG acknowledges support from the Erasmus+ traineeship program and MA from the Christiane-Nüsslein-Volhard Foundation. WBH was supported by grants from the DFG (SFB 655, A2), the ERC (250197) and ERA-NET NEURON (MicroKin).

Additional information

Funding

Funder	Grant reference number	Author
European Molecular Biology Organization	ALTF 861-2013	Nereo Kalebic
Deutsche Forschungsgemeinschaft	SFB 655, A2	Wieland B Huttner
European Research Council	250197	Wieland B Huttner
Max-Planck-Gesellschaft		Wieland B Huttner
Christiane-Nüsslein-Volhard Foundation		Mareike Albert
Erasmus+	Traineeship program	Carlotta Gilardi

The funders had no role in study design, data collection and interpretation, or the decision to submit the work for publication.

Author contributions

Nereo Kalebic, Conceptualization, Formal analysis, Investigation, Visualization, Methodology, Writing—original draft, Writing—review and editing, Performed ferret in utero electroporations; Carlotta Gilardi, Investigation, Visualization, Methodology, Assisted with ferret surgeries; Mareike Albert, Investigation, RNA isolation, RT-qPCR and gene expression analysis; Takashi Namba, Resources, ARHGAP11B construct and antibody; Katherine R Long, Milos Kostic, Methodology, Assisted with ferret surgeries; Barbara Langen, Methodology, Ferret hysterectomy, Assisted with ferret in utero electroporations; Wieland B Huttner, Conceptualization, Supervision, Funding acquisition, Project administration, Writing—review and editing

Author ORCIDs

Nereo Kalebic [id http://orcid.org/0000-0002-8445-2906](http://orcid.org/0000-0002-8445-2906)
Mareike Albert [id http://orcid.org/0000-0001-9855-9344](http://orcid.org/0000-0001-9855-9344)
Katherine R Long [id http://orcid.org/0000-0003-0660-2486](http://orcid.org/0000-0003-0660-2486)
Wieland B Huttner [id http://orcid.org/0000-0003-4143-7201](http://orcid.org/0000-0003-4143-7201)

Ethics

Animal experimentation: All experimental procedures were conducted in agreement with the German Animal Welfare Legislation after approval by the Landesdirektion Sachsen (licences TVV 2/2015 and TVV 21/2017).

Decision letter and Author response

Decision letter <https://doi.org/10.7554/eLife.41241.021>

Author response <https://doi.org/10.7554/eLife.41241.022>

Additional files

Supplementary files

- Supplementary file 1. Overview of the effects of ARHGAP11B expression on neural progenitor cells and upper-layer neurons in developing ferret neocortex. Data taken from the indicated figure panels were used for the calculations shown. For the calculations pertaining to upper-layer neurons, it is assumed that the ARHGAP11B-induced increase in the lateral length of the FP+ area in the rostro-caudal dimension is equal to that in the medio-lateral dimension (1.25-fold).
DOI: <https://doi.org/10.7554/eLife.41241.018>

- Transparent reporting form

DOI: <https://doi.org/10.7554/eLife.41241.019>

Data availability

All data generated or analysed during this study are included in the manuscript and supporting files.

References

- Alcamo EA**, Chirivella L, Dautzenberg M, Dobrev G, Fariñas I, Grosschedl R, McConnell SK. 2008. *Satb2* regulates callosal projection neuron identity in the developing cerebral cortex. *Neuron* **57**:364–377. DOI: <https://doi.org/10.1016/j.neuron.2007.12.012>, PMID: 18255030
- Arai Y**, Pulvers JN, Haffner C, Schilling B, Nüsslein I, Calegari F, Huttner WB. 2011. Neural stem and progenitor cells shorten S-phase on commitment to neuron production. *Nature Communications* **2**:154. DOI: <https://doi.org/10.1038/ncomms1155>, PMID: 21224845
- Azevedo FA**, Carvalho LR, Grinberg LT, Farfel JM, Ferretti RE, Leite RE, Jacob Filho W, Lent R, Herculano-Houzel S. 2009. Equal numbers of neuronal and nonneuronal cells make the human brain an isometrically scaled-up primate brain. *The Journal of Comparative Neurology* **513**:532–541. DOI: <https://doi.org/10.1002/cne.21974>, PMID: 19226510
- Bailey JA**, Gu Z, Clark RA, Reinert K, Samonte RV, Schwartz S, Adams MD, Myers EW, Li PW, Eichler EE. 2002. Recent segmental duplications in the human genome. *Science* **297**:1003–1007. DOI: <https://doi.org/10.1126/science.1072047>, PMID: 12169732
- Barnette AR**, Neil JJ, Kroenke CD, Griffith JL, Epstein AA, Bayly PV, Knutsen AK, Inder TE. 2009. Characterization of brain development in the ferret via MRI. *Pediatric Research* **66**:80–84. DOI: <https://doi.org/10.1203/PDR.0b013e3181a291d9>, PMID: 19287340
- Betizeau M**, Cortay V, Patti D, Pfister S, Gautier E, Bellemin-Ménard A, Afanassieff M, Huissoud C, Douglas RJ, Kennedy H, Dehay C. 2013. Precursor diversity and complexity of lineage relationships in the outer subventricular zone of the primate. *Neuron* **80**:442–457. DOI: <https://doi.org/10.1016/j.neuron.2013.09.032>, PMID: 24139044
- Bininda-Emonds OR**, Cardillo M, Jones KE, MacPhee RD, Beck RM, Grenyer R, Price SA, Vos RA, Gittleman JL, Purvis A. 2007. The delayed rise of present-day mammals. *Nature* **446**:507–512. DOI: <https://doi.org/10.1038/nature05634>, PMID: 17392779
- Borrell V**, Götz M. 2014. Role of radial glial cells in cerebral cortex folding. *Current Opinion in Neurobiology* **27**:39–46. DOI: <https://doi.org/10.1016/j.conb.2014.02.007>, PMID: 24632307
- Borrell V**, Reillo I. 2012. Emerging roles of neural stem cells in cerebral cortex development and evolution. *Developmental Neurobiology* **72**:955–971. DOI: <https://doi.org/10.1002/dneu.22013>, PMID: 22684946
- Borrell V**. 2018. How cells fold the cerebral cortex. *The Journal of Neuroscience* **38**:776–783. DOI: <https://doi.org/10.1523/JNEUROSCI.1106-17.2017>, PMID: 29367288
- Britanova O**, de Juan Romero C, Cheung A, Kwan KY, Schwark M, Gyorgy A, Vogel T, Akopov S, Mitkovski M, Agoston D, Sestan N, Molnár Z, Tarabykin V. 2008. *Satb2* is a postmitotic determinant for upper-layer neuron specification in the neocortex. *Neuron* **57**:378–392. DOI: <https://doi.org/10.1016/j.neuron.2007.12.028>, PMID: 18255031
- Dehay C**, Kennedy H, Kosik KS. 2015. The outer subventricular zone and primate-specific cortical complexification. *Neuron* **85**:683–694. DOI: <https://doi.org/10.1016/j.neuron.2014.12.060>, PMID: 25695268
- Dennis MY**, Eichler EE. 2016. Human adaptation and evolution by segmental duplication. *Current Opinion in Genetics & Development* **41**:44–52. DOI: <https://doi.org/10.1016/j.gde.2016.08.001>, PMID: 27584858
- Dennis MY**, Harshman L, Nelson BJ, Penn O, Cantsilieris S, Huddleston J, Antonacci F, Penewit K, Denman L, Raja A, Baker C, Mark K, Malig M, Janke N, Espinoza C, Stessman HAF, Nuttle X, Hoekzema K, Lindsay-Graves TA, Wilson RK, et al. 2017. The evolution and population diversity of human-specific segmental duplications. *Nature Ecology & Evolution* **1**:0069. DOI: <https://doi.org/10.1038/s41559-016-0069>
- Dominguez MH**, Ayoub AE, Rakic P. 2013. POU-III transcription factors (*Brn1*, *Brn2*, and *Oct6*) influence neurogenesis, molecular identity, and migratory destination of upper-layer cells of the cerebral cortex. *Cerebral Cortex* **23**:2632–2643. DOI: <https://doi.org/10.1093/cercor/bhs252>, PMID: 22892427
- Englund C**, Fink A, Lau C, Pham D, Daza RA, Bulfone A, Kowalczyk T, Hevner RF. 2005. *Pax6*, *Tbr2*, and *Tbr1* are expressed sequentially by radial glia, intermediate progenitor cells, and postmitotic neurons in developing neocortex. *Journal of Neuroscience* **25**:247–251. DOI: <https://doi.org/10.1523/JNEUROSCI.2899-04.2005>, PMID: 15634788
- Fame RM**, MacDonald JL, Macklis JD. 2011. Development, specification, and diversity of callosal projection neurons. *Trends in Neurosciences* **34**:41–50. DOI: <https://doi.org/10.1016/j.tins.2010.10.002>, PMID: 21129791
- Fei JF**, Haffner C, Huttner WB. 2014. 3' UTR-dependent, miR-92-mediated restriction of *Tis21* expression maintains asymmetric neural stem cell division to ensure proper neocortex size. *Cell Reports* **7**:398–411. DOI: <https://doi.org/10.1016/j.celrep.2014.03.033>, PMID: 24726360
- Fernández V**, Llinares-Benadero C, Borrell V. 2016. Cerebral cortex expansion and folding: what have we learned? *The EMBO Journal* **35**:1021–1044. DOI: <https://doi.org/10.15252/embj.201593701>, PMID: 27056680
- Fiddes IT**, Lodewijk GA, Mooring M, Bosworth CM, Ewing AD, Mantalas GL, Novak AM, van den Bout A, Bishara A, Rosenkrantz JL, Lorig-Roach R, Field AR, Haussler M, Russo L, Bhaduri A, Nowakowski TJ, Pollen AA, Dougherty ML, Nuttle X, Addor MC, et al. 2018. Human-specific *notch2nl* genes affect notch signaling and cortical neurogenesis. *Cell* **173**:1356–1369. DOI: <https://doi.org/10.1016/j.cell.2018.03.051>, PMID: 29856954

- Fietz SA**, Kelava I, Vogt J, Wilsch-Bräuninger M, Stenzel D, Fish JL, Corbeil D, Riehn A, Distler W, Nitsch R, Huttner WB. 2010. OSVZ progenitors of human and ferret neocortex are epithelial-like and expand by integrin signaling. *Nature Neuroscience* **13**:690–699. DOI: <https://doi.org/10.1038/nn.2553>, PMID: 20436478
- Florio M**, Albert M, Taverna E, Namba T, Brandl H, Lewitus E, Haffner C, Sykes A, Wong FK, Peters J, Guhr E, Klemroth S, Prüfer K, Kelso J, Naumann R, Nüsslein I, Dahl A, Lachmann R, Pääbo S, Huttner WB. 2015. Human-specific gene ARHGAP11B promotes basal progenitor amplification and neocortex expansion. *Science* **347**:1465–1470. DOI: <https://doi.org/10.1126/science.aaa1975>, PMID: 25721503
- Florio M**, Heide M, Pinson A, Brandl H, Albert M, Winkler S, Wimberger P, Huttner WB, Hiller M. 2018. Evolution and cell-type specificity of human-specific genes preferentially expressed in progenitors of fetal neocortex. *eLife* **7**:e32332. DOI: <https://doi.org/10.7554/eLife.32332>, PMID: 29561261
- Florio M**, Huttner WB. 2014. Neural progenitors, neurogenesis and the evolution of the neocortex. *Development* **141**:2182–2194. DOI: <https://doi.org/10.1242/dev.090571>, PMID: 24866113
- Florio M**, Namba T, Pääbo S, Hiller M, Huttner WB. 2016. A single splice site mutation in human-specific ARHGAP11B causes basal progenitor amplification. *Science Advances* **2**:e1601941. DOI: <https://doi.org/10.1126/sciadv.1601941>, PMID: 27957544
- Gertz CC**, Kriegstein AR. 2015. Neuronal migration dynamics in the developing ferret cortex. *Journal of Neuroscience* **35**:14307–14315. DOI: <https://doi.org/10.1523/JNEUROSCI.2198-15.2015>, PMID: 26490868
- Geschwind DH**, Rakic P. 2013. Cortical evolution: judge the brain by its cover. *Neuron* **80**:633–647. DOI: <https://doi.org/10.1016/j.neuron.2013.10.045>, PMID: 24183016
- Götz M**, Huttner WB. 2005. The cell biology of neurogenesis. *Nature Reviews Molecular Cell Biology* **6**:777–788. DOI: <https://doi.org/10.1038/nrm1739>, PMID: 16314867
- Hansen DV**, Lui JH, Parker PR, Kriegstein AR. 2010. Neurogenic radial glia in the outer subventricular zone of human neocortex. *Nature* **464**:554–561. DOI: <https://doi.org/10.1038/nature08845>, PMID: 20154730
- Haubensak W**, Attardo A, Denk W, Huttner WB. 2004. Neurons arise in the basal neuroepithelium of the early mammalian telencephalon: a major site of neurogenesis. *PNAS* **101**:3196–3201. DOI: <https://doi.org/10.1073/pnas.0308600100>, PMID: 14963232
- Herculano-Houzel S**, Catania K, Manger PR, Kaas JH. 2015. Mammalian brains are made of these: a dataset of the numbers and densities of neuronal and nonneuronal cells in the brain of glires, primates, scandentia, eulipotyphlans, afrotherians and artiodactyls, and their relationship with body mass. *Brain, Behavior and Evolution* **86**:145–163. DOI: <https://doi.org/10.1159/000437413>, PMID: 26418466
- Hutsler JJ**, Lee DG, Porter KK. 2005. Comparative analysis of cortical layering and supragranular layer enlargement in rodent carnivore and primate species. *Brain Research* **1052**:71–81. DOI: <https://doi.org/10.1016/j.brainres.2005.06.015>, PMID: 16018988
- Jackson CA**, Peduzzi JD, Hickey TL. 1989. Visual cortex development in the ferret. I. Genesis and migration of visual cortical neurons. *The Journal of Neuroscience* **9**:1242–1253. DOI: <https://doi.org/10.1523/JNEUROSCI.09-04-01242.1989>, PMID: 2703875
- Jardim-Messeder D**, Lambert K, Noctor S, Pestana FM, de Castro Leal ME, Bertelsen MF, Alagaili AN, Mohammad OB, Manger PR, Herculano-Houzel S. 2017. Dogs have the most neurons, though not the largest brain: trade-off between body mass and number of neurons in the cerebral cortex of large carnivorous species. *Frontiers in Neuroanatomy* **11**:118. DOI: <https://doi.org/10.3389/fnana.2017.00118>, PMID: 29311850
- Kaas JH**. 2013. The evolution of brains from early mammals to humans. *Wiley Interdisciplinary Reviews: Cognitive Science* **4**:33–45. DOI: <https://doi.org/10.1002/wcs.1206>, PMID: 23529256
- Kagawa Y**, Matsumoto S, Kamioka Y, Mimori K, Naito Y, Ishii T, Okuzaki D, Nishida N, Maeda S, Naito A, Kikuta J, Nishikawa K, Nishimura J, Haraguchi N, Takemasa I, Mizushima T, Ikeda M, Yamamoto H, Sekimoto M, Ishii H, et al. 2013. Cell cycle-dependent Rho GTPase activity dynamically regulates cancer cell motility and invasion in vivo. *PLoS One* **8**:e83629. DOI: <https://doi.org/10.1371/journal.pone.0083629>, PMID: 24386239
- Kalebic N**, Taverna E, Tavano S, Wong FK, Suchold D, Winkler S, Huttner WB, Sarov M. 2016. CRISPR/Cas9-induced disruption of gene expression in mouse embryonic brain and single neural stem cells in vivo. *EMBO reports* **17**:338–348. DOI: <https://doi.org/10.15252/embr.201541715>, PMID: 26758805
- Kalebic N**, Long K, Huttner WB. 2017. Neocortex expansion in development and evolution: the cell biology of neural stem and progenitor cells and the impact of human-specific gene expression. In: Kaas J (Ed). *Evolution of Nervous Systems*. 2. Oxford: Elsevier. p. 73–89. DOI: <https://doi.org/10.1016/B978-0-12-804042-3.00136-6>
- Kawasaki H**, Iwai L, Tanno K. 2012. Rapid and efficient genetic manipulation of gyrencephalic carnivores using in utero electroporation. *Molecular Brain* **5**:24. DOI: <https://doi.org/10.1186/1756-6606-5-24>, PMID: 22716093
- Kawasaki H**, Toda T, Tanno K. 2013. In vivo genetic manipulation of cortical progenitors in gyrencephalic carnivores using in utero electroporation. *Biology Open* **2**:95–100. DOI: <https://doi.org/10.1242/bio.20123160>, PMID: 23336081
- Kawasaki H**. 2014. Molecular investigations of the brain of higher mammals using gyrencephalic carnivore ferrets. *Neuroscience Research* **86**:59–65. DOI: <https://doi.org/10.1016/j.neures.2014.06.006>, PMID: 24983876
- Kolk SM**, Whitman MC, Yun ME, Shete P, Donoghue MJ. 2006. A unique subpopulation of Tbr1-expressing deep layer neurons in the developing cerebral cortex. *Molecular and Cellular Neuroscience* **32**:200–214. DOI: <https://doi.org/10.1016/j.mcn.2005.08.022>, PMID: 16858776
- Kroenke CD**, Bayly PV. 2018. How forces fold the cerebral cortex. *The Journal of Neuroscience* **38**:767–775. DOI: <https://doi.org/10.1523/JNEUROSCI.1105-17.2017>, PMID: 29367287
- Krubitzer L**. 2007. The magnificent compromise: cortical field evolution in mammals. *Neuron* **56**:201–208. DOI: <https://doi.org/10.1016/j.neuron.2007.10.002>, PMID: 17964240

- LaMonica BE**, Lui JH, Hansen DV, Kriegstein AR. 2013. Mitotic spindle orientation predicts outer radial glial cell generation in human neocortex. *Nature Communications* **4**:1665. DOI: <https://doi.org/10.1038/ncomms2647>, PMID: 23575669
- Lange C**, Huttner WB, Calegari F. 2009. Cdk4/cyclinD1 overexpression in neural stem cells shortens G1, delays neurogenesis, and promotes the generation and expansion of basal progenitors. *Cell Stem Cell* **5**:320–331. DOI: <https://doi.org/10.1016/j.stem.2009.05.026>, PMID: 19733543
- Lewitus E**, Hof PR, Sherwood CC. 2012. Phylogenetic comparison of neuron and glia densities in the primary visual cortex and hippocampus of carnivores and primates. *Evolution* **66**:2551–2563. DOI: <https://doi.org/10.1111/j.1558-5646.2012.01601.x>, PMID: 22834752
- Lewitus E**, Kelava I, Kalinka AT, Tomancak P, Huttner WB. 2014. An adaptive threshold in mammalian neocortical evolution. *PLoS Biology* **12**:e1002000. DOI: <https://doi.org/10.1371/journal.pbio.1002000>, PMID: 25405475
- Lodato S**, Arlotta P. 2015. Generating neuronal diversity in the mammalian cerebral cortex. *Annual Review of Cell and Developmental Biology* **31**:699–720. DOI: <https://doi.org/10.1146/annurev-cellbio-100814-125353>, PMID: 26359774
- López-Hidalgo M**, Hoover WB, Schummers J. 2016. Spatial organization of astrocytes in ferret visual cortex. *Journal of Comparative Neurology* **524**:3561–3576. DOI: <https://doi.org/10.1002/cne.24015>, PMID: 27072916
- Lui JH**, Hansen DV, Kriegstein AR. 2011. Development and evolution of the human neocortex. *Cell* **146**:18–36. DOI: <https://doi.org/10.1016/j.cell.2011.06.030>, PMID: 21729779
- Martínez-Martínez MÁ**, De Juan Romero C, Fernández V, Cárdenas A, Götz M, Borrell V. 2016. A restricted period for formation of outer subventricular zone defined by Cdh1 and Trnp1 levels. *Nature Communications* **7**:11812. DOI: <https://doi.org/10.1038/ncomms11812>, PMID: 27264089
- Matsumoto N**, Shinmyo Y, Ichikawa Y, Kawasaki H. 2017. Gyrfication of the cerebral cortex requires FGF signaling in the mammalian brain. *eLife* **6**:e29285. DOI: <https://doi.org/10.7554/eLife.29285>, PMID: 29132503
- McEvilly RJ**, de Diaz MO, Schonemann MD, Hooshmand F, Rosenfeld MG. 2002. Transcriptional regulation of cortical neuron migration by POU domain factors. *Science* **295**:1528–1532. DOI: <https://doi.org/10.1126/science.1067132>, PMID: 11859196
- Miyata T**, Kawaguchi A, Saito K, Kawano M, Muto T, Ogawa M. 2004. Asymmetric production of surface-dividing and non-surface-dividing cortical progenitor cells. *Development* **131**:3133–3145. DOI: <https://doi.org/10.1242/dev.01173>, PMID: 15175243
- Mo Z**, Zecevic N. 2009. Human fetal radial glia cells generate oligodendrocytes in vitro. *Glia* **57**:490–498. DOI: <https://doi.org/10.1002/glia.20775>, PMID: 18814269
- Molnár Z**, Métin C, Stoykova A, Tarabykin V, Price DJ, Francis F, Meyer G, Dehay C, Kennedy H. 2006. Comparative aspects of cerebral cortical development. *European Journal of Neuroscience* **23**:921–934. DOI: <https://doi.org/10.1111/j.1460-9568.2006.04611.x>, PMID: 16519657
- Molyneaux BJ**, Arlotta P, Menezes JR, Macklis JD. 2007. Neuronal subtype specification in the cerebral cortex. *Nature Reviews Neuroscience* **8**:427–437. DOI: <https://doi.org/10.1038/nrn2151>, PMID: 17514196
- Noctor SC**, Martínez-Cerdeño V, Ivic L, Kriegstein AR. 2004. Cortical neurons arise in symmetric and asymmetric division zones and migrate through specific phases. *Nature Neuroscience* **7**:136–144. DOI: <https://doi.org/10.1038/nn1172>, PMID: 14703572
- Nonaka-Kinoshita M**, Reillo I, Artegiani B, Martínez-Martínez MÁ, Nelson M, Borrell V, Calegari F. 2013. Regulation of cerebral cortex size and folding by expansion of basal progenitors. *The EMBO Journal* **32**:1817–1828. DOI: <https://doi.org/10.1038/emboj.2013.96>, PMID: 23624932
- Otani T**, Marchetto MC, Gage FH, Simons BD, Livesey FJ. 2016. 2D and 3D stem cell models of primate cortical development identify species-specific differences in progenitor behavior contributing to brain size. *Cell Stem Cell* **18**:467–480. DOI: <https://doi.org/10.1016/j.stem.2016.03.003>, PMID: 27049876
- Pilaz LJ**, Patti D, Marcy G, Ollier E, Pfister S, Douglas RJ, Betizeau M, Gautier E, Cortay V, Doerflinger N, Kennedy H, Dehay C. 2009. Forced G1-phase reduction alters mode of division, neuron number, and laminar phenotype in the cerebral cortex. *PNAS* **106**:21924–21929. DOI: <https://doi.org/10.1073/pnas.0909894106>, PMID: 19959663
- Pollen AA**, Nowakowski TJ, Chen J, Retallack H, Sandoval-Espinosa C, Nicholas CR, Shuga J, Liu SJ, Oldham MC, Diaz A, Lim DA, Leyrat AA, West JA, Kriegstein AR. 2015. Molecular identity of human outer radial glia during cortical development. *Cell* **163**:55–67. DOI: <https://doi.org/10.1016/j.cell.2015.09.004>, PMID: 26406371
- Poluch S**, Juliano SL. 2015. Fine-tuning of neurogenesis is essential for the evolutionary expansion of the cerebral cortex. *Cerebral Cortex* **25**:346–364. DOI: <https://doi.org/10.1093/cercor/bht232>, PMID: 23968831
- Rakic P**. 1972. Mode of cell migration to the superficial layers of fetal monkey neocortex. *The Journal of Comparative Neurology* **145**:61–83. DOI: <https://doi.org/10.1002/cne.901450105>, PMID: 4624784
- Rakic P**. 1978. Neuronal migration and contact guidance in the primate telencephalon. *Postgraduate Medical Journal* **54 Suppl 1**:25–40. PMID: 364453
- Rakic P**. 2003a. Developmental and evolutionary adaptations of cortical radial glia. *Cerebral Cortex* **13**:541–549. DOI: <https://doi.org/10.1093/cercor/13.6.541>, PMID: 12764027
- Rakic P**. 2003b. Elusive radial glial cells: historical and evolutionary perspective. *Glia* **43**:19–32. DOI: <https://doi.org/10.1002/glia.10244>, PMID: 12761862
- Rakic P**. 2009. Evolution of the neocortex: a perspective from developmental biology. *Nature Reviews Neuroscience* **10**:724–735. DOI: <https://doi.org/10.1038/nrn2719>, PMID: 19763105
- Reillo I**, de Juan Romero C, García-Cabezas MÁ, Borrell V. 2011. A role for intermediate radial glia in the tangential expansion of the mammalian cerebral cortex. *Cerebral Cortex* **21**:1674–1694. DOI: <https://doi.org/10.1093/cercor/bhq238>, PMID: 21127018

- Reillo I, Borrell V.** 2012. Germinal zones in the developing cerebral cortex of ferret: ontogeny, cell cycle kinetics, and diversity of progenitors. *Cerebral Cortex* **22**:2039–2054. DOI: <https://doi.org/10.1093/cercor/bhr284>, PMID: 21988826
- Sawada K, Watanabe M.** 2012. Development of cerebral sulci and gyri in ferrets (*Mustela putorius*). *Congenital Anomalies* **52**:168–175. DOI: <https://doi.org/10.1111/j.1741-4520.2012.00372.x>, PMID: 22925218
- Shinmyo Y, Terashita Y, Dinh Duong TA, Horiike T, Kawasumi M, Hosomichi K, Tajima A, Kawasaki H.** 2017. Folding of the cerebral cortex requires Cdk5 in upper-layer neurons in gyrencephalic mammals. *Cell Reports* **20**:2131–2143. DOI: <https://doi.org/10.1016/j.celrep.2017.08.024>, PMID: 28854363
- Shitamukai A, Konno D, Matsuzaki F.** 2011. Oblique radial glial divisions in the developing mouse neocortex induce self-renewing progenitors outside the germinal zone that resemble primate outer subventricular zone progenitors. *Journal of Neuroscience* **31**:3683–3695. DOI: <https://doi.org/10.1523/JNEUROSCI.4773-10.2011>, PMID: 21389223
- Sidman RL, Rakic P.** 1973. Neuronal migration, with special reference to developing human brain: a review. *Brain Research* **62**:1–35. DOI: [https://doi.org/10.1016/0006-8993\(73\)90617-3](https://doi.org/10.1016/0006-8993(73)90617-3), PMID: 4203033
- Smart IH, McSherry GM.** 1986a. Gyrus formation in the cerebral cortex in the ferret. I. Description of the external changes. *Journal of Anatomy* **146**:141–152. PMID: 3693054
- Smart IH, McSherry GM.** 1986b. Gyrus formation in the cerebral cortex of the ferret. II. Description of the internal histological changes. *Journal of Anatomy* **147**:27–43. PMID: 3693076
- Smart IH, Dehay C, Giroud P, Berland M, Kennedy H.** 2002. Unique morphological features of the proliferative zones and postmitotic compartments of the neural epithelium giving rise to striate and extrastriate cortex in the monkey. *Cerebral Cortex* **12**:37–53. DOI: <https://doi.org/10.1093/cercor/12.1.37>, PMID: 11734531
- Sousa AMM, Meyer KA, Santpere G, Gulden FO, Sestan N.** 2017. Evolution of the human nervous system function, structure, and development. *Cell* **170**:226–247. DOI: <https://doi.org/10.1016/j.cell.2017.06.036>, PMID: 28708995
- Sugitani Y, Nakai S, Minowa O, Nishi M, Jishage K, Kawano H, Mori K, Ogawa M, Noda T.** 2002. Brn-1 and Brn-2 share crucial roles in the production and positioning of mouse neocortical neurons. *Genes & Development* **16**:1760–1765. DOI: <https://doi.org/10.1101/gad.978002>, PMID: 12130536
- Suzuki IK, Gacquer D, Van Heurck R, Kumar D, Wojno M, Bilheu A, Herpoel A, Lambert N, Cheron J, Polleux F, Detours V, Vanderhaeghen P.** 2018. Human-specific NOTCH2NL genes expand cortical neurogenesis through delta/notch regulation. *Cell* **173**:1370–1384. DOI: <https://doi.org/10.1016/j.cell.2018.03.067>, PMID: 29856955
- Tarabykin V, Stoykova A, Usman N, Gruss P.** 2001. Cortical upper layer neurons derive from the subventricular zone as indicated by Svet1 gene expression. *Development* **128**:1983–1993. PMID: 11493521
- Tavano S, Taverna E, Kalebic N, Haffner C, Namba T, Dahl A, Wilsch-Bräuninger M, Paridaen J, Huttner WB.** 2018. Insm1 induces neural progenitor delamination in developing neocortex via downregulation of the adherens junction belt-specific protein plekha7. *Neuron* **97**:1299–1314. DOI: <https://doi.org/10.1016/j.neuron.2018.01.052>, PMID: 29503187
- Turrero García M, Chang Y, Arai Y, Huttner WB.** 2016. S-phase duration is the main target of cell cycle regulation in neural progenitors of developing ferret neocortex. *Journal of Comparative Neurology* **524**:456–470. DOI: <https://doi.org/10.1002/cne.23801>, PMID: 25963823
- Voigt T.** 1989. Development of glial cells in the cerebral wall of ferrets: direct tracing of their transformation from radial glia into astrocytes. *The Journal of Comparative Neurology* **289**:74–88. DOI: <https://doi.org/10.1002/cne.902890106>, PMID: 2808761
- Wang X, Tsai JW, LaMonica B, Kriegstein AR.** 2011. A new subtype of progenitor cell in the mouse embryonic neocortex. *Nature Neuroscience* **14**:555–561. DOI: <https://doi.org/10.1038/nn.2807>, PMID: 21478886
- Wilsch-Bräuninger M, Florio M, Huttner WB.** 2016. Neocortex expansion in development and evolution - from cell biology to single genes. *Current Opinion in Neurobiology* **39**:122–132. DOI: <https://doi.org/10.1016/j.conb.2016.05.004>, PMID: 27258840
- Wong FK, Fei JF, Mora-Bermúdez F, Taverna E, Haffner C, Fu J, Anastassiadis K, Stewart AF, Huttner WB.** 2015. Sustained pax6 expression generates primate-like basal radial glia in developing mouse neocortex. *PLOS Biology* **13**:e1002217. DOI: <https://doi.org/10.1371/journal.pbio.1002217>, PMID: 26252244